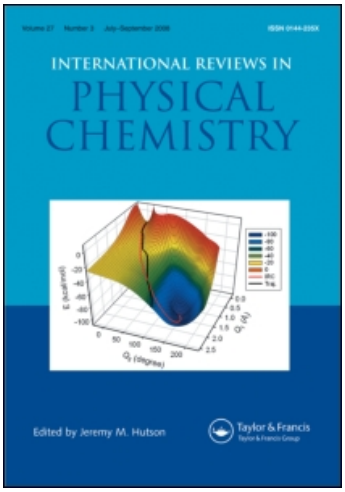

International Reviews in Physical Chemistry
Publication details, including instructions for authors and subscription information:
http://www.informaworld.com/smpp/title~content=t713724383

Production and application of translationally cold molecules

Hendrick L. Bethlem[a]; Gerard Meijer[abc]
[a] FOM-Institute for Plasma Physics Rijnhuizen, Nieuwegein, The Netherlands [b] Department of Molecular and Laser Physics, University of Nijmegen, Nijmegen, The Netherlands [c] Fritz Haber Institut-Max-Planck-Gesellschaft, Berlin, Germany

Online publication date: 26 November 2010

To cite this Article Bethlem, Hendrick L. and Meijer, Gerard(2003) 'Production and application of translationally cold molecules', International Reviews in Physical Chemistry, 22: 1, 73 — 128
To link to this Article: DOI: 10.1080/0144235021000046422
URL: http://dx.doi.org/10.1080/0144235021000046422

INT. REVIEWS IN PHYSICAL CHEMISTRY, 2003
VOL. 22, NO. 1, 73–128

Taylor & Francis
Taylor & Francis Group

Production and application of translationally cold molecules

HENDRICK L. BETHLEM
FOM-Institute for Plasma Physics Rijnhuizen, P.O. Box 1207, NL-3430 BE Nieuwegein, The Netherlands.

and GERARD MEIJER
FOM-Institute for Plasma Physics Rijnhuizen, P.O. Box 1207, NL-3430 BE Nieuwegein, The Netherlands, Department of Molecular and Laser Physics, University of Nijmegen, Toernooiveld 1, NL-6525 ED Nijmegen, The Netherlands, and Fritz Haber Institut-Max-Planck-Gesellschaft, Faradayweg 4-6, D-14195 Berlin, Germany

Inspired by the spectacular successes in the field of cold atoms, there is currently great interest in cold molecules. Cooling molecules is useful for various fundamental physics studies and gives access to an exotic regime in chemistry where the wave property of the molecules becomes important. Although cooling molecules has turned out to be considerably more difficult than cooling atoms, a number of methods to produce samples of cold molecules have been demonstrated over the last few years. This paper aims to review the application of cold molecules and the methods to produce them. Emphasis is put on the deceleration of polar molecules using time-varying electric fields. The operation principle of the array of electrodes that is used to decelerate polar molecules is described in analogy with, and using terminology from, charged-particle accelerators. It is shown that, by applying an appropriately timed high voltage burst, molecules can be decelerated while the phase-space density, i.e. the number of molecules per position–velocity interval, remains constant. In this way the high density and low temperature in the moving frame of a pulsed molecular beam can be transferred to the laboratory frame. Experiments on metastable CO in states that are either repelled by or attracted to high electric fields are presented. Loading of slow molecules into traps and storage rings is discussed.

Contents

International Reviews in Physical Chemistry ISSN 0144–235X print/ISSN 1366–591X online © 2003 Taylor & Francis Ltd
http://www.tandf.co.uk/journals
DOI: 10.1080/0144235021000046422

1. Introduction

Over the last two decades, physicists have steadily learned to control the motion of particles, ranging from neutrons to ions, atoms and finally molecules. These methods have led to a renaissance in atomic physics and have the potential to do the same for molecular physics. Ultracold atoms are used in time standards and in precision tests of quantum electrodynamics and various other fundamental physics theories. Atom cooling methods have also made possible the realization of Bose–Einstein condensation in dilute atomic vapours and the atom laser. Not surprisingly, physicists and chemists now want to perform the same tricks with molecules. However, molecules have much more to offer than simply extending the experiments already performed with atoms to more complex species. For instance, the dipole–dipole interaction in a molecular Bose–Einstein condensate gives a molecular condensate new and intriguing properties. Polar Fermi gases may be used to observe

the superfluid transition. Cooling molecules will also make it possible to improve the resolution of various fundamental physics studies. For instance, specific molecules such as YbF and PbO are considered ideal for testing the time reversal symmetry postulate and chiral molecules are being used to study parity violation. Furthermore, cold molecules offer various interesting possibilities for chemistry. Cooling molecules to ultracold temperatures gives access to an exotic regime for chemical reactivity, where the thermal de Broglie wavelength exceeds the size of the collision complex. Similarly, the formation of long-lived, transiently bound molecular complexes enables reactions to occur via tunnelling through reaction barriers, thus opening novel routes for low-temperature chemistry. This paper aims to review the application of cold molecules and the methods to produce them. Three methods have been successfully applied to produce translationally cold molecules. In the first technique diatomic molecules are formed by the association of cold atoms using photons as the necessary third body. In the second technique molecules are cooled via collisions with a helium buffer gas in a cryogenic cell. In the third technique time-varying electric fields are used to decelerate a pulsed molecular beam. In this paper the last method, which has been developed in our laboratory, will be emphasized. For earlier reviews on cold molecules see Masnou-Seeuws and Pillet (2001) and Bahns *et al*. (2000). A popular scientific report has appeared in Goss Levi (2000).

Our paper is organized as follows. In section 2 the motivation for studying cold molecules is made more explicit. In section 3 an overview is given of methods to produce cold molecules. To set the stage and to give the reader a feel for the numbers involved, atom cooling experiments are discussed first in this section. In section 4 the interaction between molecules and electric fields is outlined. In section 5 deceleration of a beam of metastable CO is presented, using molecules in states which are either repelled by or attracted to high electric fields. Finally, in section 6 trapping and storing polar molecules is discussed.

2. Applications of cold molecules

Almost all of our knowledge of atoms and molecules has been acquired through either (i) spectroscopy or (ii) collision studies. Lowering the temperature of the atoms or molecules to be studied has a profound impact on both approaches. The following discussion will emphasize applications which cannot, or cannot easily, be performed using cold atoms. Some experiments discussed here might already be possible with the densities and temperatures achieved in our laboratory. Some other applications, however, require cooling to significantly lower temperatures. Whether these experiments turn out to be feasible depends on whether techniques such as evaporative cooling and sympathetic cooling will prove to be as effective for molecules as they have been for atoms.

2.1. *High-resolution spectroscopy*

At room temperature the average velocity of gas-phase molecules is about $500\,\mathrm{m\,s^{-1}}$. These high velocities limit our ability to study the molecules. Ultimately, the resolution of molecular spectroscopy is limited by the time the molecule spends in the measuring device. In a common apparatus the time one has to study a molecule will be limited to a few milliseconds, which in turn limits the width of the observed spectral line to a few kHz. At a temperature of 25 mK ammonia molecules have an average velocity of $5\,\mathrm{m\,s^{-1}}$. Cooling the molecules down to millikelvin temperatures,

therefore, improves the attainable resolution by orders of magnitude. Besides the interaction time, the resolution depends on the number of molecules that are detected; if too much signal is lost this will be the bottleneck in the experiment. In most cases the improved resolution will not justify the trouble associated with cooling molecules. However, there are a number of cases in which it is needed to have the highest possible resolution, and some of these are outlined below.

2.1.1. *Time reversal symmetry violation*

At very high precision an atom or molecule is no longer adequately described as a system containing protons, neutrons and electrons only. Rather, it is necessary to include a sea of virtual particles surrounding them, allowed to exist, for very short times, by the Heisenberg uncertainty principle. Therefore, by performing very sensitive spectroscopic measurements we can learn how these virtual particles interact with the constituents of an atom or a molecule. This ushers atomic and molecular physics into an area which has traditionally been reserved to particle physicists. Of particular interest are interactions which lead to a non-zero electric dipole moment (EDM) of an electron and of other elementary particles. The dipole moment is a measure for the charge distribution of the particle. Since the electron is assumed to be a point charge, however, the EDM is considered to be a measure of the average displacement of the electron charge from the electron's centre of mass. An EDM would imply an asymmetry with respect to time reversal (T), commonly referred to as T-violation. So far, the only system known to violate T is the neutral kaon. T-violation has deep consequences for the evolution of the universe, in particular the question of baryon asymmetry (i.e. the fact that the universe seems to be built almost entirely out of matter, where one might expect an equal distribution of matter and antimatter). According to the standard model, the EDM of the electron is too small to be detected by any currently conceivable method. However, it is generally believed that the standard model is incomplete, and extensions to the standard model predict considerably larger values for the electron dipole moment, comparable with, or larger than, the current experimental upper limit. Increasing the experimental accuracy may therefore make it possible either to exclude these theories or to see evidence for physics beyond the standard model (Hunter 1991, Hinds and Sauer 1997).

A possible EDM of the electron necessarily lies along the angular momentum axis. If it were to lie along a different axis we would have to require a new quantum number to describe the projection of the EDM along the angular momentum axis ('EDM up' or 'EDM down'). In that case Pauli's exclusion principle would allow us to store twice as many electrons in each shell as we observe. The EDM can therefore be measured by orienting the angular momentum axis with respect to an auxiliary electric field and looking for a difference in energy on reversing the polarity of the electric field. Obviously, we cannot perform this measurement on a free electron as it would crash into the electrodes immediately. A possible way out of this difficulty is to measure the permanent EDM of a neutral atom or molecule† having an unpaired

† This is not to be confused with the (induced) electric dipole moment of a polar molecule. The shift in energy due to the interaction between an electric dipole moment of a polar molecule and an external electric field is quadratic at sufficiently small electric fields. The shift due to the interaction of a permanent EDM with an external field, on the other hand, is linear at small electric fields and therefore depends on the direction of the electric field as well as on its absolute size.

electron and then attempt to interpret the result in terms of the free electron. Intuitively we would expect the applied electric field to be screened completely by the other charges in the atom or molecule and, therefore, the atom or molecule to have no permanent EDM, even though its constituents do. This is indeed true for a point particle in a non-relativistic limit; however, in high-Z atoms and molecules the electrons move at very high velocities in the vicinity of the nucleus, and relativistic properties are in fact very important. In this case the effective electric field on the electron can actually be much larger than the applied field. The auxiliary field is used merely to orient this internal electric field with respect to the laboratory frame (Schiff 1963, Sandars 1965). Note that the EDM of an atom or molecule can be induced by T-violating interactions between its constituents even in the absence of intrinsic EDMs.

We can express the effective electric field experienced by the unpaired electron in an atom or molecule in the form $\varepsilon_{\text{eff}} = QP$, where Q is a factor which includes all details of the atomic or molecular structure (including relativistic effects) and P is the degree of polarization of the system by the external field. For Q typical values for both atoms and molecules are $Q \sim (10\text{–}100) \times 10^9\,\text{V cm}^{-1} \times (Z/80)^3$; the dependence on the mass number, Z, reflects the fact that both the electric fields and the relativistic effects are large in the vicinity of heavy nuclei (DeMille *et al.* 2000). Q is similar for both atoms and molecules. Since polar molecules are readily polarized in an electric field, P is $\sim$1 at modest external electric fields. For atoms, however, P is 100–1000 times smaller even at the highest attainable electric fields. The effective electric field on an electron in a molecule is therefore 100–1000 times larger than on an electron in an atom.

The sensitivity of any experiment searching for an EDM depends both on the size of the energy shift, $\Delta E = |\mathbf{d}_e \varepsilon_{\text{eff}}|$, with d_e the size of the EDM and ε_{eff} the effective electric field, and on the ability to measure this shift. The most accurate experiment on the EDM of the electron until now has been performed on atoms (Regan *et al.* 2002), for which much more sensitive techniques are available. It is expected, however, that ultimately the huge internal fields available in polar molecules will be decisive and that the most sensitive measurement of the EDM will be performed on a molecule (Hudson *et al.* 2002). The ability to cool the molecules down to millikelvin temperatures will improve the resolution by orders of magnitude (Egorov *et al.* 2001).

2.1.2. *Parity-violating interaction in chiral molecules*

Chiral molecules occur in two forms which are mirror images of one another and cannot be superimposed. Naively, one would expect these so-called enantiomers to be identical in all their behaviour. There is in fact a large difference in the biochemical properties of left- and right-handed enantiomers. All living organisms contain left-handed amino acids only. It may be asked, therefore, whether there is an intrinsic difference between the chemical properties of the enantiomers which gives rise to the preference of one particular form in chemical reactions. This difference, however small, might have caused a full selection of one enantiomer in the millennia that have evolved since the first appearance of living organisms on Earth. The only interaction known to violate mirror symmetry, referred to as parity violation, is the weak interaction. An energy difference between the right- and left-handed molecules would therefore be a manifestation of the weak interaction in molecules (Rein 1974, Letokhov 1975).

The simplest chiral molecule one could think of is NHDT, an isotopomer of ammonia. Unfortunately, this molecule is radioactive and therefore troublesome to work with. Furthermore, the energy difference is expected to be larger for molecules having at least one heavy atom on the periphery. The most sensitive measurement up to now has been performed on CHFClBr. In this experiment the spectra of the two enantiomers of CHFClBr are recorded simultaneously in a twin cavity (Daussy *et al.* 1999, Ziskind *et al.* 2002). The resolution is currently limited by chemical impurities in the cell. It is expected that the next experiment will be performed using a molecular beam. The ability to decelerate this beam will improve the resolution further.

2.1.3. *Time dependence of fundamental constants*

Time is the most accurately measured quantity in nature. Since 1967 the second has been defined as 9 192 631 770 periods of the radiation correponding to the transition between two hyperfine states in ^{133}Cs. Atomic frequency standards are, therefore, casually referred to as atomic clocks (Jones 2000). Interesting physics can be performed by comparing two atomic clocks. For instance the time variation of the fine structure constant α can be tested by simultaneously measuring transitions with a different dependence on α. Temporal changes of α would result in a shift between the ratio of two measured frequencies as a function of time. Variation of fundamental constants may be expected as a consequence of the expanding universe (Webb *et al.* 2001).

The long lifetime of vibrationally excited states in molecules makes vibrational transitions very suitable for metrology purposes. A test of the time dependence of α could be performed by phase-coherent comparison between an electronic and a vibrational transition in a trapped molecule (Ye 2002).

2.1.4. *Lifetime measurements*

Besides the energy of a level, an interesting quantity of a state is its lifetime. Conventional molecular beam techniques limit the determination of lifetimes up to a few milliseconds. By storing molecules in a trap much longer lifetimes can be measured. This makes it possible to study the lifetimes of vibrationally or electronically excited metastable states. Molecules can be prepared in these states either in a trap or prior to deceleration. By measuring the trap-loss spectrum, transitions can be measured which are difficult to detect otherwise.

2.2. *Cold collisions*

2.2.1. *Quantum chemistry*

At the end of the 19th century, it was thought that there was a qualitative difference between light, described as waves, and atoms and molecules, described as particles. However, this difference was only an appearance. Under certain conditions, light behaves like particles, as was shown in 1905 by Albert Einstein. Conversely, under certain conditions particles behave like waves, as was shown by Louis de Broglie in 1923. The extent to which molecules behave as a wave depends on their temperature. At room temperature the length of the wave which is associated with an ammonia molecule is 0.23 Å, much smaller than the (classical) separation between the nitrogen atom and the hydrogen atoms which make up the ammonia molecule. At 25 mK the associated wavelength is 25 Å, considerably larger than this separation. Therefore, the classic picture of a molecule which rolls like a

marble on the potential energy surface needs radical modification. Rather, ultracold collisions are more accurately described as interfering waves (Herschbach 1999, Balakrishnan and Dalgarno 2001).

Besides studying cold collisions in a static sample of molecules, cold collisions can also be studied using a crossed molecular beam set-up. The ability to tune the molecular beam velocity allows collision cross-sections to be determined as a function of the collision energy. Interesting effects are predicted for collisions at small but non-zero collision energies. Calculations show that elastic and inelastic cross-sections exhibit sharp resonances at low collision energies (0–100 cm^{-1}), the cross-section increasing by two orders of magnitude at these energies (Balakrishnan *et al.* 2000). In particular unusual resonant states can be formed when the colliding molecules begin to rotate, leaving them with insufficient translational energy to overcome their van der Waals attraction. These resonances are foreign to cold atom–atom collisions since they arise from the rearrangement of rotational energy; at low enough temperatures, translational energy is transferred by the anisotropy of the potential energy surface into rotational energy, effectively binding the molecules transiently together. This type of resonance is ubiquitous in cold molecule–molecule collisions because the enormous number of internal molecular states leads to an equally large number of resonant states. Measurement of this predicted structure yields unprecedented opportunities to investigate fine details of the potential energy surface of the interacting species, giving complementary information to conventional spectroscopy of collision complexes (Heijmen *et al.* 1999, Balakrishnan *et al.* 2000).

2.2.2. *Quantum degenerate gases*

When a particle is trapped, its de Broglie wave is reflected by the walls of the trap and interferes with itself. As a consequence, the particle is no longer able to have just any velocity it chooses; only certain discrete energies are allowed. At elevated temperatures these discrete energies lie infinitesimally close to each other. At very low temperatures, however, the separation between the levels becomes significant and only the lowest few levels in the trap are populated. A very interesting situation occurs when the de Broglie wavelength of a group of particles is larger than the mean particle separation. In that case the outcome depends on whether the particles obey Bose–Einstein or Fermi–Dirac statistics. When the particles are bosons (consisting of an even number of constituents; neutrons, protons and electrons) they prefer to populate the same state. If we cool down a trapped bosonic gas, all particles will, at some point, suddenly occupy the lowest trap state. This transition is called Bose–Einstein condensation (BEC) and was first observed in 1995 in a gas of rubidium atoms (Anderson *et al.* 1995). A Bose–Einstein condensate has some very intriguing properties. Since all atoms are in the same quantum state, they are indistinguishable; not just in practice, but fundamentally, they have become some sort of a super-atom. When, on the other hand, the particles are fermions (consisting of an odd number of constituents; neutrons, protons and electrons) each level in the trap can be occupied by one particle only. When we cool down a trapped fermionic gas, at some point all states up to a certain temperature will be filled. When the gas is then further cooled, the cloud can no longer shrink owing to the 'Fermi pressure' resulting from the Pauli exclusion principle. This has recently been observed in a lithium gas (Truscott *et al.* 2001).

The most interesting property of degenerate quantum gases is that, although the atoms behave fully quantum-mechanically, the cloud of atoms is in fact a few

micrometres in size. If a degenerate molecular gas is formed there is the possibility of studying its behaviour for molecules in selected vibrational and (end-over-end) rotational states. Arguably, the most interesting aspect of molecules compared with atoms is their dipole–dipole interaction.

2.2.3. *Dipole–dipole interaction*

Two molecules having an electric dipole moment of 1 Debye, spaced at a distance of 1 μm, have an interaction energy corresponding to 170 nK. Depending on the relative orientation of these dipoles this interaction is attractive or repulsive. At very low temperature, when the translational energy becomes comparable with the dipole–dipole interaction energy, the trapped molecules influence each others' trajectories. It is predicted that the molecules will form a dipolar crystal analogous to an ionic crystal in ion traps (Shlyapnikov 2001).

The dipole–dipole interaction also dramatically changes the properties of a degenerate gas (Baranov *et al.* 2002b). All experiments on BEC so far are well described by the Gross–Pitaevskii equation. This equation incorporates all atom–atom interactions in the so-called mean field interparticle interaction, given by $4\pi\hbar^2 a/m$ times the number of atoms, with a being the scattering length. When the interaction is repulsive (positive scattering length), the BEC will be stable for any number of atoms. When the interaction is attractive (negative scattering length) the BEC will be stable only for a condensate with a limited number of atoms, as is the case for ^{7}Li and ^{85}Rb. For all atomic species thus far condensed the (magnetic) dipole–dipole interaction can be neglected compared with the contact potential (Góral *et al.* 2000). The electric dipole–dipole interaction is, however, typically 3 orders of magnitude stronger than its magnetic counterpart, and dominates the interaction. In a polarized polar gas the interaction depends on the geometry of the trap. In a cigar-shaped trap along the direction of polarization of the molecules, the interaction is mainly attractive. Conversely, in pancake-shaped traps the interaction is mainly repulsive. By changing the geometry of the trap one therefore has a knob to tune the interaction in the gas, thus offering new possibilities for controlling and engineering macroscopic quantum states (Santos *et al.* 2000).

The interaction in the gas plays a decisive role in Fermi gases. When a Fermi gas is cooled below the Fermi temperature, the cloud can no longer shrink. It is proposed, however, that at a certain temperature the cloud may collapse owing to interparticle interactions. The fermions will form pairs which behave as pseudo-bosons. This is the standard Bardeen–Cooper–Schrieffer (BCS) theory of superconductivity in metals. Because of the Pauli principle, the interaction between identical fermions vanishes at ultracold temperatures. In order to observe the superfluid transition in dilute atomic gases one therefore needs simultaneous trapping of at least two different fermionic species. The constraint on the relative concentrations of these species is rather severe. Ultracold polar gases, on the other hand, interact via dipole–dipole interactions, which are energy independent in the ultracold limit. Therefore, the BCS transitions can be obtained in a single-component polar Fermi gas. For $^{15}ND_3$ the transition is predicted to occur at temperatures higher than 100 nK at a density of $> 5 \times 10^{12}$ molecules cm^{-3} (Baranov *et al.* 2002a).

Another interesting area of research is the interaction between trapped dipoles in an optical lattice. Depending on the exact geometry of the lattice, the dipoles will be ordered according to a certain pattern. The long-range character of the dipole–dipole

interactions allows for the existence of not only Mott-insulating and superfluid phases, which have been observed recently in an atomic gas (Greiner *et al*. 2002), but also several other phases such as supersolid, checkerboard and collapse phases (Góral *et al*. 2002). The possibility of tuning the interaction may permit an experimental realization of all these different phases, which would also allow for a detailed experimental study of quantum phase transitions. Polar molecules in an optical lattice might also be used in quantum computation; in this design, the qubits, the quantum equivalent of a bit, are the EDMs of ultracold molecules, oriented along or against an external electric field. Coupling between the bits occurs via the electric dipole–dipole interaction (DeMille 2002).

3. Cooling techniques

In a conservative system, the density and temperature of a group of particles are coupled through the Liouville theorem; lowering of the temperature can be accomplished by an accompanying decrease in density only. The number of molecules per space interval (density) and velocity interval (temperature) is referred to as the phase-space density. Techniques which lower the temperature of a gas and lead to an increase of the phase-space density are referred to as real cooling, as opposed to cooling techniques which only lower the temperature at the expense of the density.

We will use as the definition of the phase-space density,

$$D = n\Lambda^3, \tag{1}$$

where n is the number density and $\Lambda = \left(2\pi\hbar^2/mkT\right)^{1/2}$ is the thermal de Broglie wavelength. This quantity is sometimes referred to as the degeneracy parameter of a gas. The degeneracy parameter is a measure of the de Broglie wavelength of the particles, expressed in terms of the particles' separation. In the Boltzmann regime (far from quantum degeneracy, $D \ll 1$), the degeneracy parameter is equal to the number of molecules per space and velocity interval, and thus equivalent to the definition of phase-space density in classical mechanics.

3.1. *Atom cooling*

3.1.1. *Laser cooling*

Over recent decades, immense progress has been made in gaining control over the motion of neutral atoms. These developments have been made possible by the use of laser cooling (Chu 1998, Cohen-Tannoudji 1998, Phillips 1998); atoms are cooled by many consecutive absorption–emission cycles leading to a significant momentum transfer from the photons in the laser beam to the atom. Spontaneous emission acts as a friction force, damping the motion of the atoms and thereby increasing their phase-space density. Using normal laser-cooling techniques, atoms are routinely cooled to temperatures below 1 mK (70 μK for Rb) at a density of 10^{10} atoms cm^{-3}, or more. By using techniques such as polarization gradient cooling even lower temperatures can be obtained (7 μK for Rb). The number of atoms and the density are limited by radiation trapping of the cooling light and by excited-state collisions. To avoid these limitations traps are used which keep the atoms in so-called 'dark' hyperfine states for most of the time. This allows for a confinement of 10^{10} atoms at a density of 10^{12} atoms cm^{-3} (Metcalf and van der Straten 1999).

3.1.2. *Evaporative cooling*

When a gas is confined at a sufficiently high density, the collisions in the trapped gas will (tend to) establish a thermodynamic equilibrium. The energy distribution of the particles is given by a Boltzmann distribution. However, in a trap with a finite depth, a certain fraction of the atoms have an energy which exceeds the trap depth. These atoms will escape from the trap. Since the atoms which are expelled have a higher energy than the average, the temperature will be decreased when a new equilibrium is established, etc. The rate of the evaporative cooling depends on the number of elastic collisions in the gas, and thus on the density, and on the depth of the trap (ϵ_T) compared with the temperature (T) of the trapped gas ($\eta = \epsilon_T/kT$). The evaporation must compete with heating processes such as inelastic relaxation and collisions with background gas. By keeping η fixed (for instance by lowering the frequency of a microwave knife which limits the trap depth by inducing transitions to untrapped states) the density will increase and so will the rate of evaporative cooling. This is termed run-away evaporative cooling. In this way the phase-space density increases considerably (Ketterle and van Druten 1996). This has been the final step in experiments which have led to BEC in alkali gases (and hydrogen). In the first demonstration of BEC at JILA in 1995, 4×10^6 rubidium atoms were laser cooled to a temperature of 90 μK at a peak density of 4×10^{10} atoms cm^{-3}, corresponding to a phase-space density of 3×10^{-7}. After an evaporation sweep of 70 s, the BEC transition took place, with 2×10^4 atoms at a peak density of 3×10^{12} atoms cm^{-3} and a temperature of 170 nK (Anderson *et al.* 1995). Since the first demonstration, numerous other groups have succeeded in obtaining BEC. BEC has now been observed in ^{1}H, ^{4}He*, ^{7}Li, ^{23}Na, ^{41}K, ^{85}Rb and ^{87}Rb. Potassium is a particular interesting case: because of its less than ideal electronic structure, the phase-space density of laser-cooled potassium is (~100 times) too small to allow for evaporative cooling towards BEC. Even so, BEC has recently been achieved by sympathetically cooling potassium atoms with rubidium atoms (Modugno *et al.* 2001).

3.2. *Molecular cooling*

Extending the laser-cooling techniques to molecules is very difficult. Laser cooling requires a 'simple' energy level structure, making it possible to cycle a transition a large number of times without off-resonant fluorescence. This excludes most atoms and all molecules. The problem is not due to the rotation of the molecule; transitions between different rotational states are governed by strict selection rules, and for a variety of molecules transitions can be found that are rotationally and electronically closed. The problem is due to the vibration of the molecule, as transitions between different vibrational states are governed by Franck–Condon factors, i.e. the overlap of the corresponding vibrational wavefunctions. After spontaneous emission molecules therefore generally end up distributed over a large number of vibrational states. A possible exception to this might be the NH radical which has a transition around 337 nm with a Franck–Condon factor better than 0.999 (van de Meerakker *et al.* 2001). IR transitions are considered to be too weak for effective laser cooling.

Because of these problems, molecules have long been regarded as not amenable to cooling and trapping experiments. In 1998, 13 years after the first neutral atoms were trapped (Migdall *et al.* 1985), two different methods were demonstrated to cool and trap molecules (Weinstein *et al.* 1998a, Takekoshi *et al.* 1998).

3.2.1. *Buffer-gas cooling*

Cryogenic methods have been used to cool hydrogen to millikelvin temperatures since the 1970s. Buffer-gas cooling can be applied to hydrogen because hydrogen has a very small binding energy to a helium (covered) surface. All other atoms or molecules, except for helium, will stick to the walls at these temperatures. At temperatures of a few hundred millikelvin helium still has quite a high vapour pressure, high enough to be used as a buffer gas. If other atoms or molecules are introduced into the cryogenic cell they will be cooled by the helium vapour to low enough temperatures to make them trappable in a superconducting magnetic trap. In order to ensure that the atoms or molecules thermalize before impinging on the walls of the cryogenic cell surrounding the trap, the density of the buffer gas needs to be large enough to allow for thermalization on a length scale smaller than the size of the cell. This puts a lower limit on the temperature of the buffer gas. For ^{3}He and ^{4}He, temperatures as low as 240 mK and 800 mK can be used respectively for a cell on the order of 1 cm. Buffer-gas cooling has been developed by the group of Doyle at Harvard (Doyle *et al.* 1995, Friedrich *et al.* 1998). About 1×10^{12} europium (Kim *et al.* 1997) or chromium (Weinstein *et al.* 1998b) atoms were loaded into a magnetic trap at a peak density of 5×10^{12} atoms cm^{-3} and at a temperature of around 300 mK. Using the same technique, the group reported trapping of about 10^8 CaH molecules at a density of 8×10^7 molecules cm^{-3} and at a temperature of 400 mK (Weinstein *et al.* 1998a). Buffer-gas cooling and trapping is applicable to any paramagnetic molecule (or atom) provided that a means is available to introduce the molecule into the cryogenic cell. So far, laser ablation of a solid precursor has been used. A more general way might be to couple an atomic or molecular beam into the cryogenic cell (Egorov *et al.* 2002). In this way a larger number of molecules might be trapped. In order to obtain a truly isolated sample of cold molecules, the buffer gas needs to be rapidly pumped out after loading of the trap. This has already been demonstrated for europium and chromium, but for CaH the 1/e lifetime of the trapped molecules is only 0.6 s, shorter than the time currently needed to pump away the buffer gas (about 20 s) (deCarvalho *et al.* 1999). This rather short trapping lifetime is attributed to evaporation (low η) of CaH molecules over the edge of the trap.† This is less of a problem for europium and chromium for which the trap is much deeper (high η); europium and chromium have a magnetic dipole moment of 7 and 6 Bohr magneton, respectively, while CaH has a magnetic dipole moment of only 1 Bohr magneton.

3.2.2. *Association of cold atoms*

The problems of cooling molecules can be avoided by forming molecules from laser-cooled atoms. Because of energy and momentum conservation, two colliding atoms can only form a molecule if a third particle is present. In a photoassociation process, two atoms resonantly absorb one photon to form a molecule in a rovibrational level of an electronically excited state (Thorsheim *et al.* 1987). In this way ultracold H_2 (Mosk *et al.* 1999), He_2^* (Herschbach *et al.* 2000), Li_2 (Abraham *et al.* 1995), Na_2 (Lett *et al.* 1993), K_2 (Nikolov *et al.* 1999), Ca_2 (Zinner *et al.* 2000), Rb_2 (Miller *et al.* 1993, Gabbanini *et al.* 2000) and Cs_2 (Fioretti *et al.* 1998) have

† In this case, evaporation does not lead to a decrease of the temperature since the molecules are still in thermal contact with the walls of the cryogenic cell.

been formed. The formation of molecules is deduced from an observed reduction in the number of trapped atoms as a function of the wavelength of the photoassociation laser. In some cases, the molecules produced have also been detected directly (Fioretti *et al.* 1998, Nikolov *et al.* 1999, Gabbanini *et al.* 2000). The photoassociation spectrum exhibits lines of a sharpness comparable with bound–bound transitions, and so the formation of molecules can be very efficient. However, the lifetime of a photoassociated molecule is short, and after a few nanoseconds the molecule will decay by spontaneous emission, usually giving back a pair of atoms. Crucial to the formation of stable molecules is the branching ratio between bound–bound and bound–free transitions. Favourable cases are Cs_2 and Rb_2, that, because of the existence of a double-well structure in long-range excited states, have a fairly large Franck–Condon overlap at short internuclear distances. Formation rates of up to 0.2 molecules per second per atom have been obtained (Drag *et al.* 2000). Similar formation rates have been observed for K_2 using a more elaborate scheme (Nikolov *et al.* 2000). The translational temperature of the molecules can be as low as that of the atoms from which they are formed. The cold molecular sample formed after spontaneous emission of the photoassociated molecules is in a statistical mixture of different rovibrational levels. In order to obtain molecules in a single state (preferably the ground state), stimulated Raman schemes have been applied (Laburthe Tolra *et al.* 2001). Formation of mixed-alkali species is also being pursued (Schaffer *et al.* 1999), but has turned out to be considerably more difficult because of a less favourable Franck–Condon overlap for the free–bound transition. The formation of $^6Li^7Li$ has been demonstrated unambiguously (Schlöder *et al.* 2001).

Recently, photoassociation of atoms has been demonstrated in a Bose–Einstein condensate (Wynar *et al.* 2000, Gerton *et al.* 2000, McKenzie *et al.* 2002). The group of Heinzen has observed free–bound stimulated Raman transitions with a linewidth as small as 1.5 kHz (Wynar *et al.* 2000). This provides the possibility to couple an atomic condensate to a molecular condensate; the matter analogue of frequency doubling of laser light. The group of Wieman has produced coherent coupling between atoms and molecules in an ^{85}Rb condensate using a time-varying magnetic field near a Feshbach resonance (Donley *et al.* 2002). A Feshbach resonance is a scattering resonance for which the total energy of two colliding atoms just matches the energy of a bound molecular state. The atoms and molecules generally have a different magnetic moment and the difference depends on the magnetic field strength. Therefore by changing the duration and magnitude of the magnetic field the amount of coupling between the atoms and molecules is tuned (Zoller 2002). The group of Wieman observed oscillations in the number of atoms in the atomic BEC which they interpreted as an oscillation between an atomic and molecular condensate. Since the molecules formed are highly excited (the distance between the atoms in the molecules is essentially the same as their distance in the condensate) they are likely to undergo an inelastic collision with an atom in the condensate. In order to obtain a stable molecular condensate it is necessary to bring the molecules down to their rovibrational ground state (Kokkelmans *et al.* 2001).

Once formed, the molecules can be trapped in a number of ways. The group of Knize first demonstrated trapping of molecules that were formed from laser-cooled atoms (Takekoshi *et al.* 1998). Using an intense CO_2 laser they managed to trap a small number of Cs dimers. More recently the groups of Pillet (Vanhaecke *et al.* 2002) and Heinzen (Heinzen *et al.* 2002) have reported magnetic trapping of

photoassociated molecules. Vanhaecke *et al.* (2002) reported trapping of about 1×10^5 molecules at a temperature below 100 μK.

3.2.3. *Molecular beam deceleration*

A powerful and general method to cool a gas is by letting it expand through a nozzle into vacuum. Let us consider a container with a high pressure gas (typically 1–5 atm). In the container there is a small hole through which the molecules emerge into vacuum, as shown in figure 1. If the hole is much smaller than the mean free path of the gas (the mean distance that a molecule travels before it collides with another molecule) the velocity distribution inside the container will not be disturbed. Every now and then molecules escape through the hole, without suffering from collisions while they leave the container. The velocity distribution in the beam is the same as it was in the container. These beams are said to be effusive.

If, on the other hand, the orifice is much larger than the mean free path, the situation is drastically changed. Molecules escaping through the hole collide frequently. Molecules close to the hole no longer suffer from collisions from the right, where the molecules that just escaped through the hole used to be. They will, however, still collide with molecules to the left of them. Therefore, the molecules experience a net force pushing them to the right (towards the hole). The molecules in the beam no longer have the same speed distribution as in the container; during the expansion the faster molecules collide with slower molecules flying ahead, and the average velocity in the beam is faster than the average velocity in an effusive beam. The velocity distribution is also narrower, corresponding to a lower temperature.

We can describe the expansion in terms of a hydrodynamic flow. Since the expansion occurs rapidly, it can be assumed to be adiabatic. The total energy of a mole of gas is the sum of the translational energy, K, the internal energy, U (vibrational and rotational energy), the potential energy pV, and the kinetic flow

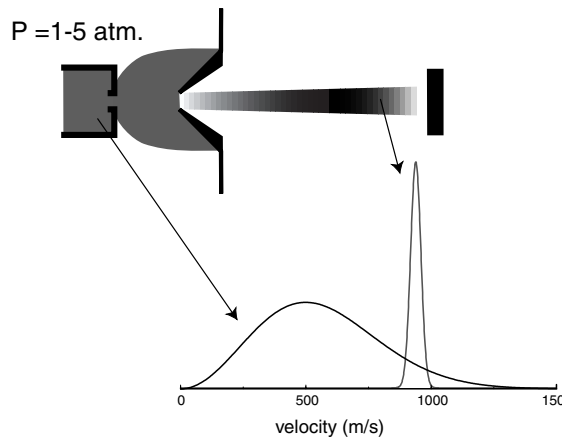

Figure 1. Schematic view of a supersonic expansion. A high-pressure gas is expanded through a small hole into vacuum. The inset shows the velocity distribution of room-temperature ammonia molecules in the container and in the supersonic beam. By using a noble gas as carrier the velocity distribution is further narrowed. The terminal velocity of the ammonia molecules will then be the same as that of the carrier gas (2000 m s^{-1} for He, 340 m s^{-1} for Xe).

energy $\frac{1}{2}M\bar{v}^2$, which will be constant during the expansion. The pressure in the beam is much smaller than in the container. Therefore,

$$K_0 + U_0 + p_0V_0 = K + U + \tfrac{1}{2}M\bar{v}^2, \tag{2}$$

where the zero subscripts denote quantities in the container.

Ultimately, all energy is converted into kinetic flow energy, implying a translational temperature equal to zero in the moving frame of the molecular beam. In reality, the temperature is limited owing to finite collision cross-sections and the formation of clusters. By the formation of clusters energy is released which will heat the beam. Cluster formation can be reduced by using a noble gas as carrier gas. Noble gases cluster only at very low temperatures and act as a heat sink in the expansion. Best results are obtained using a mixture of a few per cent of the molecules of interest in the carrier gas. In this way translational temperatures below 1 K and rotational temperatures below 5 K can be obtained. The vibrational temperatures are higher, typically some 50 K. It is interesting to note that these numbers are lower than one would expect from values of the elastic and inelastic cross-sections at room temperature; as the temperature in the beam drops, the cross-sections will increase, increasing the number of collisions that take place. The terminal velocity of the beam, determined by the carrier gas, is usually faster than the local speed of sound (therefore, the expansion is said to be supersonic). For a pulsed beam this has as a consequence that disturbances at the end of the beam cannot influence the beam that has already formed.

Let us calculate the evolution of the phase-space density in the beam. Since the expansion is assumed to be isentropic, the following relation holds:

$$n = n_0\left(\frac{T}{T_0}\right)^{1/(\gamma-1)}, \tag{3}$$

where T_0, n_0 and T, n are the temperature and number density in the container and in the beam respectively and γ is the Poisson coefficient (Reif 1965, Miller 1988). We can use this relation to calculate the phase-space density before and after the expansion. Using equation (1), we find

$$D = n\left(\frac{2\pi\hbar^2}{mkT}\right)^{3/2} = n_0\left(\frac{T}{T_0}\right)^{1/(\gamma-1)}\left(\frac{2\pi\hbar^2}{mkT}\right)^{3/2}. \tag{4}$$

For a monoatomic gas $\gamma = 5/3$, and we find that the phase-space density remains constant throughout the expansion. Molecules have internal degrees of freedom and, therefore, a smaller γ. For small molecules, such as CO and NH_3, the population in the excited vibrational levels can be neglected and we need to account for their rotational degrees of freedom only. For NH_3 at room temperature $\gamma = 9/7$, and we find that the phase-space density decreases as $(T/T_0)^2$. Here γ is assumed to be independent of temperature. For an expansion of pure ammonia we therefore expect a decrease in phase-space density of more than 3 orders of magnitude. This is the phase-space density integrated over all levels. In the expansion the rotational temperature decreases and the population in the lowest levels increases. The decrease in phase-space density is merely a compensation for the entropy decrease which is associated with this rotational cooling.

Let us now turn to a seeded beam. If the fraction of the seed gas is small the heat released by the seed gas can be neglected, and, therefore, the temperature and density

in the seeded beam are essentially the same as those in an unseeded beam. In this case the phase-space density of the seed gas integrated over all levels is approximately the same as in the container (using an average value for γ we find for a 1% mixture a phase-space density decrease of 4%; for a 15% mixture the phase-space density in the beam is 2 times lower than in the container). The phase-space density of molecules in the rotational ground state will greatly increase. Let us calculate the expected phase-space density of a mixture of 1% deuterated ammonia in 1.5 atm xenon at a temperature of 200 K (see section 6). Using $P = nkT$, we find a density of ammonia molecules in the container of 5.5×10^{17} molecules cm^{-3}. At 200 K, $\Lambda = 0.28$ Å, and thus the phase-space density of ND_3 integrated over all levels is 1.2×10^{-8}. In the beam the translational temperature of the beam is around 1 K. At this temperature, $\Lambda = 3.9$ Å, and we expect a density of 2.0×10^{14} molecules cm^{-3}. Only the lowest rotational levels will be populated in the beam. Roughly 20% of the ammonia molecules will be in the $|J = 1, MK = -1\rangle$ state, implying a phase-space density of ND_3 molecules in this quantum state of 2.5×10^{-9}. In Bethlem *et al.* (2000b, 2002b) and Crompvoets *et al.* (2001) experiments are described in which molecules in this state are decelerated and trapped. These experiments are briefly described in section 6.

Various methods are currently being explored to translate the high phase-space densities from the moving frame of the molecular beam to the laboratory frame. One method that has been demonstrated by Gupta and Herschbach (1999, 2001) uses a counter-rotating beam source. By letting the rotor spin at a suitable rate the velocity of the beam is largely cancelled, and a beam is produced which travels in the laboratory frame with a speed of a few tens of metres per second. In this way beams of CH_3F, O_2 and SF_6 have been produced with mean velocities of 91 m s^{-1}, 67 m s^{-1} and 55 m s^{-1} respectively. These velocities correspond to a temperature in the laboratory frame of 17 K, 8.6 K and 27 K respectively. The phase-space density that is obtained depends on the stagnation pressure and the temperature of the source. The centrifugal action of the rotating nozzle significantly enhances the pressure of the gas, which is, however, limited by the available pumping capacity. Gupta and Herschbach use continuous beams for which the peak density is typically 1000 times lower than for pulsed beams.

Another method that has been proposed is trapping of molecules in the focus of an intense laser beam which moves along with the molecular beam, either literally, by using a scoop (Friedrich 2000), or effectively, by using a moving standing wave (Corkum *et al.* 1999, Barker and Schneider 2001). By gradually lowering the velocity of the laser trap, the molecules can be decelerated. This method is particularly suited for highly polarizable molecules such as I_2.

The following sections describe the use of time-varying electric fields to decelerate a supersonic beam of polar molecules.

4. Manipulation of polar molecules using time-varying electric fields

Polar molecules are molecules having an asymmetric charge distribution, with one end of the molecule more positively and one end more negatively charged. This charge separation leads to a so-called electric dipole moment. The interaction of the dipole moment with an external electric field is known as the Stark effect. In this section it is shown how the Stark effect can be used to manipulate neutral molecules.

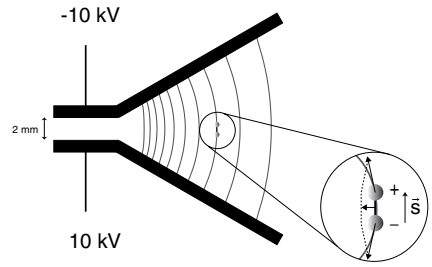

Figure 2. A dipole in the inhomogeneous electric field of a wedge. When the dipole is oriented along the electric field lines there is a net force acting on the dipole directed towards the higher electric field.

4.1. *The force on a polar molecule*

In figure 2 a classical dipole is sketched in the field formed by two wedged field plates. Lines of equal electric field are indicated. The dipole can be regarded as a positive and a negative charge q separated by a distance s. The dipole moment is then defined as $\boldsymbol{\mu} = q\mathbf{s}$, pointing from the negative to the positive charge. The separation can be quite significant on a molecular scale. For instance, the dipole moment of metastable CO is 1.37 D (4.6×10^{-30} C m), corresponding to a unit charge separation of 0.3 Å. This may be compared with the mean separation of 1 Å between the C and O atoms which make up the CO molecule. The two charges of the dipole are attracted and repelled by the electric field. When the field is inhomogeneous, these forces will not cancel exactly. The resultant force on the molecule will depend on the orientation of the dipole with respect to the electric field,

$$\mathbf{F}(\mathbf{r}) = q\left[\mathbf{E}(\mathbf{r} + \tfrac{1}{2}\mathbf{s}) - \mathbf{E}(\mathbf{r} - \tfrac{1}{2}\mathbf{s})\right] = \mu \cos\theta \nabla |\mathbf{E}(\mathbf{r})|, \tag{5}$$

with θ the angle between the dipole and the electric field lines and r the position of the dipole. In figure 2 the dipole is oriented along the field lines. In this case the resultant force is towards the higher electric field. Similarly, we see that when the dipole is oriented antiparallel to the field the resultant force is towards the lower electric field. Since the resultant force depends on the variation of the electric field over s, the force is much smaller than the force on a charged particle. In the situation depicted in figure 2 the force on either end of the dipole is 6.4×10^5 aN. Taking for instance the dipole moment of metastable CO, the resultant force is 4×10^{-3} aN, corresponding to an acceleration of $\sim 9000g$. Apart from a force on the centre of mass, the dipoles experience a torque trying to orient the dipoles parallel to the field lines. A classical dipole would, therefore, start to librate along the direction of the electric field lines.

The description so far has been purely classical. Quantum mechanics tells us that the orientation angle of the dipole moment of a molecule with respect to an external electric field can take only certain expectation values. This is known as space quantization. Space quantization was demonstrated in 1922 by Stern and Gerlach in their seminal experiment†. Apart from being the first experiment where neutral particles are manipulated using external fields, this experiment forms the starting point of the molecular beam method.

† For a review of the Stern-Gerlach experiments see Friedrich and Herschbach (1998).

4.2. *Deflection and focusing of polar molecules*

Since the average angle θ between the dipole and an external electric field is fixed, we can introduce an effective dipole moment $\mu_{\text{eff}}(|\mathbf{E}|) = \mu\overline{\cos\theta}$, which is an inherent property of the quantum state. The force on the dipole becomes

$$\mathbf{F}(\mathbf{r}) = \mu_{\text{eff}}(|\mathbf{E}|)\nabla|\mathbf{E}(\mathbf{r})|, \tag{6}$$

and its potential energy

$$W = -\mu_{\text{eff}}(|\mathbf{E}|)|\mathbf{E}(\mathbf{r})|, \tag{7}$$

which is known as the Stark shift. There is a great similarity between the acceleration of a charged particle in an electric field and the acceleration of a dipolar molecule in an inhomogeneous electric field. We can regard the effective dipole moment as analogous to the 'charge' of a dipolar molecule in the electric field. When μ_{eff} is positive the molecules are attracted to high electric fields ('high-field seekers') and when negative the molecules are repelled from high electric fields ('low-field seekers').

Inhomogeneous electric fields can therefore be used to select molecules in specific states. This has been used to perform scattering experiments with state-selected beams and to perform very sensitive microwave spectroscopy†. Inhomogeneous deflection fields act as a filter, rejecting molecules in unwanted states, but this does not lead to enhancement of the signal due to molecules in the selected state. An important improvement, therefore, was the use of magnetic and electrostatic lenses, focusing molecules in a selected state. Magnetic focusing was first performed by Friedburg and Paul (1950, 1951). Electrostatic focusing was developed independently by Gordon *et al.* (1954, 1955) and by Bennewitz *et al.* (1955). Townes and coworkers succeeded in obtaining a sufficiently high density of state-selected ammonia molecules to achieve microwave amplification by stimulated emission of radiation (MASER).

An electrostatic focuser consists of a number of rods placed equidistantly on the outside of a circle. The rods are alternately at ground potential and at high voltage, creating an electric field that is zero at the molecular beam axis and increasing further outside. Molecules in low-field-seeking states will therefore experience a force towards the molecular beam axis. Generally, the field in an n-pole is proportional to $r^{(n/2)-1}$ (Reuss 1988), where r is the distance from the molecular beam axis. Molecules with a linear Stark effect will thus experience a linear force in a hexapole. A hexapole serves as a positive lens for molecules in low-field-seeking states; molecules in high-field-seeking states, on the other hand, are defocused.

Multipole fields focus molecules in low-field-seeking states. Focusing of molecules in high-field-seeking states is more difficult. Maxwell's equations do not allow for a maximum of an electric field in free space (Wing 1984, Ketterle and Pritchard 1992), and, therefore, molecules in high-field-seeking states have a tendency to crash into the electrodes, where the electric fields are the highest. A number of schemes have been demonstrated to overcome this difficulty (Lainé and Sweeting 1973). Although it is not possible to have simultaneous focusing of molecules in high-field-seeking states in two directions, it is possible to produce a field which has a maximum in one direction and a minimum in the other direction. By alternating the orientation of these fields it is possible to obtain net focusing ('alternate gradient (AG) focusing') in either direction (Auerbach *et al.* 1966). AG focusing of polar

† For a review of state selection by magnetic and electric fields see Reuss (1988).

molecules was experimentally demonstrated by Kakati and Lainé (1967, 1969, 1971), by Günther and coworkers (Günther and Schügerl 1972, Lübbert *et al.* 1975, 1978), and by Wharton and colleagues (Bromberg 1972). Another scheme uses the fact that the electric field between two coaxial electrodes scales with distance r from the axis as $1/r$. Therefore molecules having a linear (negative) Stark shift experience a force that is proportional to $1/r^2$ and will perform stable Kepler orbits around the central electrode. This has been used by Helmer *et al.* (1960), by Chien *et al.* (1974) and, more recently, by Loesch (Loesch 1996, Loesch and Scheel 2000) to focus molecules in high-field-seeking states.

4.3. *Deceleration of polar molecules*

Molecules can be deflected and focused using fields that are inhomogeneous perpendicular to the molecular beam direction. If the electric field is inhomogeneous in the direction of the molecular beam, the longitudinal velocity of the beam will be altered. Let us consider two parallel electrodes oriented perpendicular to the molecular beam axis with a voltage difference between them (see figure 3). A molecule in a low-field-seeking state will decelerate while entering this field. If we do nothing, the molecule will accelerate while leaving the field. If, however, the electric field is greatly reduced before the molecule has left the electric field the molecule will keep its lower velocity. This process may be repeated by letting the molecules pass through multiple pulsed electric fields. Molecules can thus be slowed down and eventually brought to a standstill. This idea was first considered by King (King and Zacharias 1958, King 1959), by Oraevskiĭ (1964) and by Kazachok (1965) as a possible method to obtain MASER radiation with a reduced linewidth. The group of King at MIT constructed a 20 cm long array consisting of nine deceleration stages, intended to decelerate a beam of ammonia in the $J = 1$, $K = 1$ upper inversion level from 208 m s^{-1} to 35 m s^{-1} (Golub 1967). Each deceleration stage consisted of two parallel plates spaced 1 mm apart, having a voltage difference of 30 kV. Unfortunately, the beam intensity, at the design input velocity, was

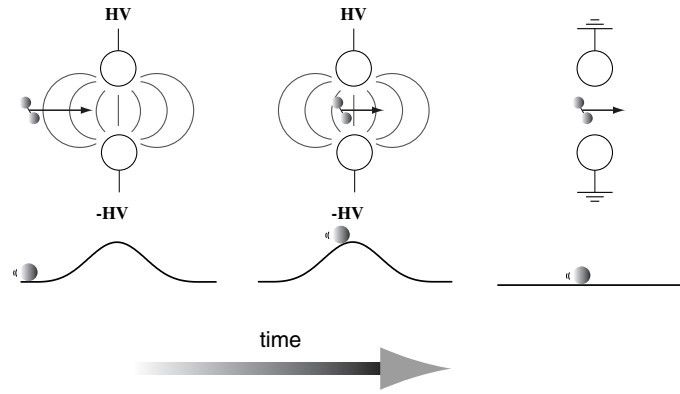

Figure 3. A polar molecule which has its dipole oriented antiparallel to the electric field lines will gain potential energy while flying into an electric field. This gain is compensated by a loss in kinetic energy; the molecule is decelerated. If a DC electric field is applied, the molecule will accelerate while leaving the electric field and regains its lost energy. However, if the electric field is abruptly switched off the molecule will keep its lower velocity.

insufficient to yield a detectable signal. The decelerator was to be operated at a constant frequency of the electric fields while the distance between adjacent plates was adjusted to compensate for the decreasing velocity of the beam. Therefore, the use of a higher input velocity required a drastic modification of the set-up, which was not undertaken. Meanwhile the interest in MASER sources was reduced owing to the invention of the laser. In 1966 a group led by Lennard Wharton at the University of Chicago† designed and constructed an 11 m long array, consisting of 600 acceleration stages intended to accelerate LiF in high-field-seeking states from 0.2 eV ($1070\,m\,s^{-1}$) to 2 eV ($3430\,m\,s^{-1}$) (Auerbach *et al.* 1966, Wolfgang 1968). Each acceleration stage consisted of two hemispherically ended rods with a diameter of 0.5 mm spaced 0.5 mm apart. The beam was focused using additional AG lenses at DC electric fields. The accelerator was designed to be operated at maximum electric fields of $850\,kV\,cm^{-1}$ and $500\,kV\,cm^{-1}$ at the acceleration stages and at the lenses respectively. These values were determined as feasible from initial tests on prototype electrodes. Unfortunately, the actual electrodes were able to withstand fields up to only 1/4 of these values, probably because of some damage to the electrodes during assembly. Initial testing of the accelerator was performed at these reduced electric field strengths. A lower initial velocity of the beam and a lower frequency of the electric field was used to compensate for the reduced acceleration per stage. The full machine was built but the tests were performed using a part of the array only (60 acceleration stages). Although AG focusing proved to work, the group was unable to demonstrate acceleration of molecules. This failure was explained by misalignments in the acceleration and lens array, in combination with a decreased acceptance due to the reduced electric field strengths used (Bromberg 1972). The project was terminated in 1972. Meanwhile the advent of supersonic nozzles had made the accelerator obsolete.

We recently implemented the first successful decelerator for neutral molecules (Bethlem *et al.* 1999)‡. A beam of metastable CO molecules in low-field-seeking states was decelerated from $230\,m\,s^{-1}$ to $98\,m\,s^{-1}$ using 63 deceleration stages. In Bethlem *et al.* (2000a) a theoretical model of the deceleration process is presented and tested. In Bethlem *et al.* (2002a) a beam of metastable CO molecules in high-field-seeking states was decelerated using 12 electrodes in AG configuration. In Bethlem *et al.* (2000b) ammonia molecules were decelerated and loaded in an electrostatic quadrupole trap, discussed at length in Bethlem *et al.* (2002b). In Crompvoets *et al.* (2001) a prototype electrostatic storage ring for neutral molecules has been demonstrated. In Crompvoets *et al.* (2002) longitudinal focusing of a beam of ammonia molecules is presented. We will here review our work on metastable CO. In section 6 the trapping and storing experiments will be briefly described.

† Apparently, Wharton (chemist) was unaware of the earlier work by King (physicist).

‡ Shortly after this work, an article was published by the group of Gould at Lawrence Berkeley National Lab (Maddi *et al.* 1999) in which they presented data on the deceleration of Cs atoms using time-varying electric fields. Since the Stark effect in atoms is weak, the deceleration they obtained was rather small. The main goal of their work was to show the prospects for decelerating polar molecules. Time-varying magnetic fields have been used to manipulate atoms (Maréchal 1999) and neutrons (Niel and Rauch 1989). Since magnetic fields cannot be switched at high frequency, time-varying magnetic fields cannot easily be applied to supersonic beams.

4.4. *Stark effect in metastable CO*

In this section we will calculate the Stark shift and the effective dipole moment of metastable CO molecules. CO in its electronic ground state has only a small dipole moment (0.1 D) and, as the ground state is a $^1\Sigma^+$ state, does not exhibit a first-order Stark effect. CO in its lowest triplet state, the metastable $a^3\Pi$ state, on the other hand, does have a relatively large dipole moment (1.37 D) and a linear Stark effect for fields over a few kV cm^{-1}. The lowest rotational state in the $\Omega = 1$ multiplet has a lifetime of 3.7 ms (Jongma *et al.* 1997b). This state can be directly laser excited from the ground state at 206 nm.

CO in the $a^3\Pi$ state has an unpaired electron leading to a non-zero electronic orbital angular momentum **L**. **L** couples to the spin–orbital angular momentum, **S**, and to the rotational angular momentum, **R**. For low rotational levels, the $a^3\Pi$ state is best described in a Hund's case (a) coupling scheme, with the good quantum numbers Λ and Σ, the projection of **L** and **S** on the molecular axis respectively. The projections of the total angular momentum **J** on the molecular axis and on the space-fixed axis also commute leading to the good quantum numbers Ω and M. In the $a^3\Pi$ state $\Omega = \Lambda + \Sigma$ can take on the possible values $0, \pm 1, \pm 2$. The projection of **R** on the molecular axis is zero by definition. The basis functions become $|n\Lambda\rangle|S\Sigma\rangle|J\Omega M\rangle|v\rangle$, representing the electronic orbital, electronic spin, rotational and vibrational components of the wavefunction respectively. The rotational part of the wavefunction contains information on how the molecular axis (and therefore the dipole moment) is oriented in the laboratory frame. In the absence of an external electric (or magnetic) field there is no preferred direction in space, and the wavefunctions must be (anti-) symmetric with respect to inversion in the molecular frame (parity). Eigenfunctions with a definite parity can be constructed from linear combinations of $|J\Omega M\rangle$ and $|J - \Omega M\rangle$ basis functions. The separation of the electronic motion and nuclear motion (Born–Oppenheimer approximation) is not exact; as the CO molecule rotates the electrons do not follow the nuclear motion exactly. This leads to a splitting of the parity states, termed Λ doubling. In the $J = 1$, $\Omega = 1$ level of the $a^3\Pi$ state, the splitting is 394 MHz. In an electric field the levels of opposite parity of a specific J level mix, leading to a first-order Stark shift. At higher electric field strengths the levels of the same parity in neighbouring J levels mix and the molecular rotation becomes hindered. Coupling of the different rotational levels leads to second- and higher-order Stark shifts.

In order to determine the Stark shift of metastable CO, the excitation spectrum is measured as a function of the electric field in which the metastable state is prepared (Jongma *et al.* 1997a). The used radiation is obtained via frequency tripling of the output of a pulsed dye amplified CW ring dye laser system. This system produces pulses of 5 ns duration with a typical energy of 1 mJ/pulse around 206 nm in a 150 MHz bandwidth. With this laser system the spin-forbidden $a^3\Pi_1 \leftarrow X^1\Sigma^+$ transition can be fully saturated. Excitation is performed on the $R_2(0)$ or on the $Q_2(1)$ line to prepare either Λ doublet component of the $a^3\Pi_1$ ($v = 0$, $J = 1$) level. The excitation is performed in a homogeneous DC electric field that is applied between two parallel, gold-coated electrodes placed 2.06 ± 0.01 mm apart. The angle between the polarization vector of the laser and the electric field is close to the magic angle of 54.7°, so that all M sublevels in the excited state are equally populated after excitation.

Figure 4 shows a number of excitation spectra in the vicinity of the $a^3\Pi_1$ ($v = 0$, $J = 1$) $\leftarrow X^1\Sigma^+$ ($v = 0$, $J = 0$) transition for different strengths of the electric field.

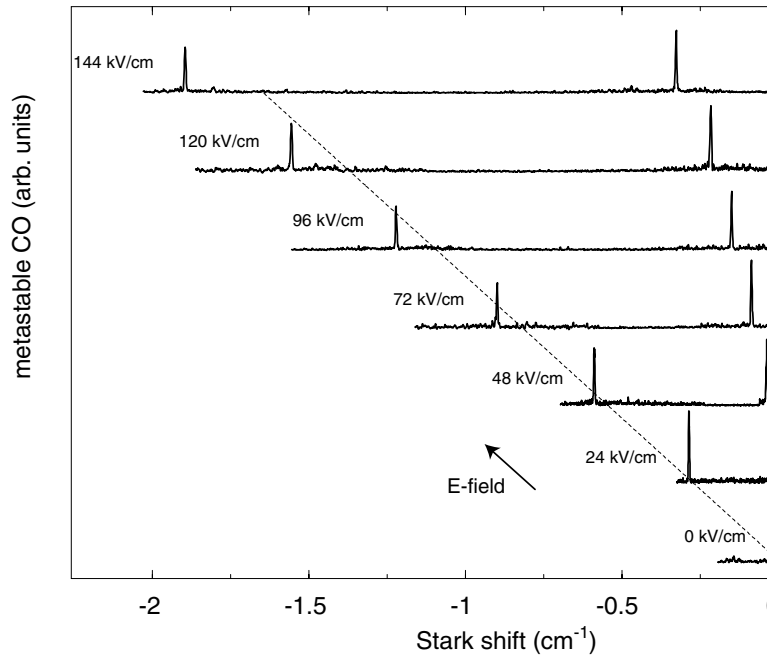

Figure 4. Excitation spectra recorded for the lower Λ doublet component of the $a^3\Pi_1(v = 0, J = 1)$ level for several values of the electric field. The horizontal axis shows the shift of the $M = 0$ and $M\Omega = 1$ level relative to the position of these levels in zero electric field. The broken line shows the calculated first-order Stark effect for the $M\Omega = 1$ level. (Figure reproduced from Jongma (1997) with permission.)

Using this transition the lower Λ doublet component of the $a^3\Pi_1$ ($v = 0$, $J = 1$) level is populated. Since the Stark shift of the ground state is negligible on this scale, the observed shifts can be interpreted as the Stark shift of the $a^3\Pi$ state. Similar spectra are measured for the $a^3\Pi_1$ ($v = 0$, $J = 1$) $\leftarrow X^1\Sigma^+$ ($v = 0$, $J = 1$) transition by which the upper Λ doublet component of the $a^3\Pi_1$ ($v = 0$, $J = 1$) level is reached.

In figure 5 the measured Stark shift is shown as a function of the applied electric field (upper panel) for both Λ doublet components. The smooth curves show the calculated Stark shift of the different components, obtained using the known value of the dipole moment and the rotational energy level structure (Field *et al.* 1972) in the $a^3\Pi$ state. The energy matrix used in the calculations includes coupling to rotational levels up to $J = 10$ for all of the three Ω ladders. The wavefunction used in this description is a superposition of the pure Hund's case (a) wavefunctions†.

The only non-zero matrix elements for the Stark energy operator H_{St} in the pure Hund's case (a) description are given by

$$\langle J, M, \Omega, \pm|H_{\mathrm{St}}|J, M, \Omega, \mp\rangle = -\frac{|M\Omega|}{J(J+1)}\mu|\mathbf{E}|, \tag{8}$$

$$\langle J, M, \Omega, \pm|H_{\mathrm{St}}|J+1, M, \Omega, \pm\rangle = -\frac{\mu|\mathbf{E}|}{J+1}\sqrt{\frac{[(J+1)^2 - \Omega^2][(J+1)^2 - M^2]}{(2J+1)(2J+3)}}, \tag{9}$$

† The procedure is explained in Jongma *et al.* (1997a).

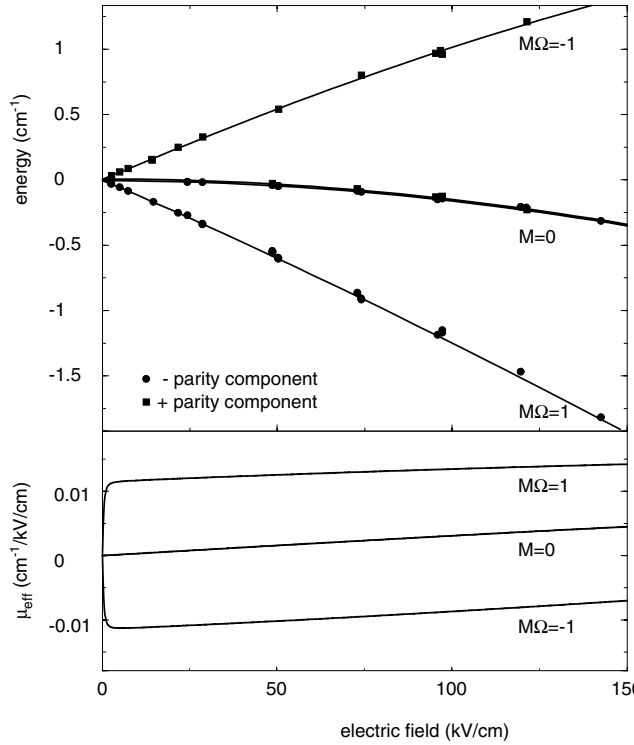

Figure 5. Measured splitting of the different M components of the CO $a^3\Pi_1(v = 0, J = 1)$ Λ doublet as a function of the applied electric field (upper panel). The vertical axis shows the position of the energy levels relative to the centre of the Λ doublet in zero electric field. The full curves show the calculated Stark shift. By dividing these curves by the electric field and multiplying by –1, the effective dipole moment is found (lower panel). (Figure reproduced from Jongma *et al.* (1997a) with permission. Copyright Elsevier Science.)

where μ is the electric dipole moment and $|\mathbf{E}|$ is the strength of the electric field. Equation (8) couples the two Λ doublet components for a specific J level in pure Hund's case (a). Because the magnitude of the Λ doubling, ΔE_Λ, is small, this term, which is responsible for the first-order Stark effect, has a large influence. Equation (9) couples two neighbouring rotational levels, which are much further apart than the two Λ doublet components, and is responsible for the second- and higher-order Stark effect. Diagonalization of the Stark energy matrix provides the eigenvalues presented for different electric field strengths in figure 5.

For low fields the second-order Stark shift can be neglected and the Stark shift takes the approximate form

$$\Delta W_{\text{Stark}} = \pm\sqrt{\left(\frac{\Delta E_\Lambda}{2}\right)^2 + \left[\mu|\mathbf{E}|\frac{M\Omega}{J(J+1)}\right]^2}, \tag{10}$$

with the plus and minus sign used for the low-field- and high-field-seeking states respectively.

By dividing the Stark curves shown in figure 5 by the electric field and multiplying by -1, we find the effective dipole moments (figure 5, lower panel).

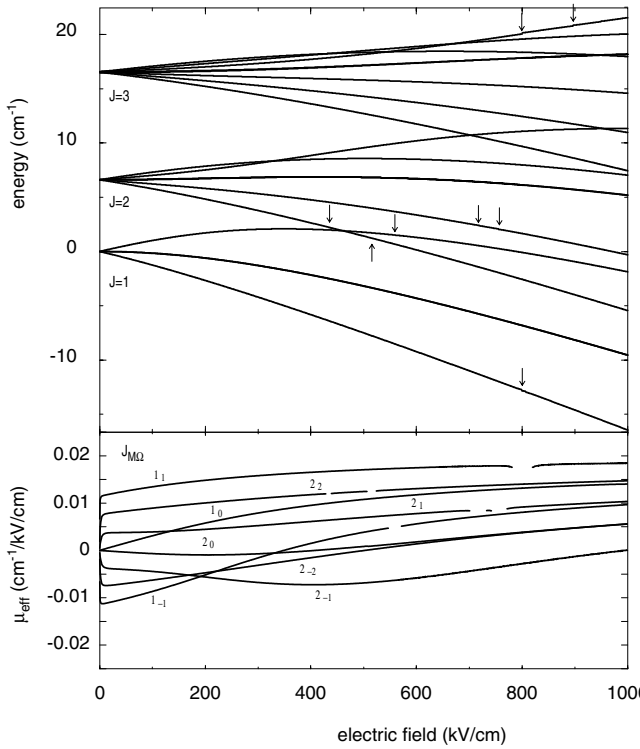

Figure 6. Calculated Stark shift of the rotational levels up to $J = 3$ of the $a^3\Pi_1(v = 0)$ state of CO in high electric fields. The vertical axis shows the position of the energy levels relative to the origin of the $J = 1$ Λ doublet of the $\Omega = 1$ ladder in zero electric field. For extremely high electric fields the existence of pendular states is observed. The discontinuities (indicated by the horizontal arrows) are due to avoided crossings with the $\Omega = 0$ and $\Omega = 2$ spin components. The lower panel shows the effective dipole moments of the $J = 1$ and $J = 2$ levels.

The calculations are performed for higher fields than can be attained experimentally as well. The results of these calculations are shown for the lowest rotational levels of the F_2 component (mainly $\Omega = 1$ character) in figure 6. The figure shows the energy of all of the $M\Omega$ components for rotational levels up to $J = 3$. The Λ doubling is too small to be seen on this scale. It is clear from the figure that levels with equal $|M\Omega|$ but different J repel each other. At high electric fields, the J levels are fully mixed, and all levels shift to lower energy. At this point the molecule no longer rotates freely but only librates about the electric field direction. These states are therefore termed 'pendular states' (Loesch and Remscheid 1990, Friedrich and Herschbach 1991). In the limit of high electric field, different states with even or odd $|M|$ correspond to different harmonic librator states with a definite orientation (and μ_{eff}) as can be seen in the lower part of figure 6. The electric fields at which J mixing takes place depend on the ratio of the dipole moment to the rotational constant of the molecule. Therefore, for heavy molecules (with relatively small rotational constants) this takes place at rather low electric fields. In table 1 the Stark shifts of a number of polar molecules are listed, together with some relevant molecular properties, such as the dipole

Table 1. A selection of polar molecules with their relevant properties.

Molecule	State	Stark shift (cm^{-1}) at 200 kV cm^{-1}	μ (D)	A, B, C (cm^{-1})	m (amu)
CO ($a^3\Pi_1$)[a]	$\|J=1, M\Omega=-1\rangle$	1.71	1.37	—, 1.68, —	28
	$\|J=1, M\Omega=+1\rangle$	−2.66			
NH_3[b]	$\|J=1, MK=-1\rangle$	2.11	1.47	—, 9.95, 6.23	17
	$\|J=1, MK=+1\rangle$	−2.19			
ND_3[c]	$\|J=1, MK=-1\rangle$	2.29	1.50	—, 5.14, 3.12	20
	$\|J=1, MK=+1\rangle$	−2.66			
OH[d]	$\|J=3/2, M\Omega=-9/4\rangle$	3.22	1.67	—, 18.5, —	17
	$\|J=3/2, M\Omega=+9/4\rangle$	−3.31			
H_2O[e]	$\|J_{K_aK_c}\|M\|\rangle = \|1_{10}1\rangle$	0.45	1.82	27.3, 14.6, 9.5	18
	$\|J_{K_aK_c}\|M\|\rangle = \|0_{00}0\rangle$	−0.34	1.85		
Pyridazine[f]	$\|J_{K_aK_c}\|M\|\rangle = \|1_{10}1\rangle$	0.13 at 9.2 kV cm^{-1}	4.14	0.21, 0.20, 0.10	80
	$\|J_{K_aK_c}\|M\|\rangle = \|0_{00}0\rangle$	−11.95			
YbF[g]	$\|J=3/2, M\Omega=-3/4\rangle$	0.3 at 20 kV cm^{-1}	3.91	—, 0.24, —	193
	$\|J=1/2, M\Omega=+1/4\rangle$	−10.9			

For details see
[a] Jongma *et al.* (1997 a),
[b] Gandhi and Bernstein (1987),
[c] Baugh *et al.* (1994),
[d] Schreel *et al.* (1993),
[e] Bulthuis *et al.* (1997),
[f] Li *et al.* (1998) and
[g] Sauer *et al.* (1996).

moments, rotational constants and mass. In Bethlem *et al.* (2002b) a more extensive list is presented.

5. Decelerating polar molecules

5.1. *Decelerating low-field seekers*

As explained in the previous section, electric fields can be used to manipulate the trajectories of neutral molecules. Static electric fields have been used to focus and deflect polar molecules while time-varying electric fields can be used to change the longitudinal velocity of polar molecules. The amount of energy that can be taken from or added to the molecule is given by the Stark shift, which can be regarded as the potential energy of the molecule in an electric field. For typical molecules this shift is a few cm^{-1} in the maximum electric fields that can be applied (see table 1). This may be compared with the kinetic energy of molecules in a supersonic beam which is typically on the order of 100 cm^{-1}. In order to make a significant change in energy we therefore need to use multiple pulsed electric fields.

It is necessary to keep the molecules together throughout the deceleration process. In this section we will discuss the stability properties of an array of electric fields. It is shown that the principle of 'phase stability', that forms the basis for synchrotron-like charged particle accelerators, can be applied to Stark deceleration as well. Phase stability was independently discovered by Veksler (1945) and McMillan (1945) and can be viewed as trapping of the particles in a travelling

potential well formed by the electric fields (Humphries 1986). By slowly decreasing the velocity of the travelling well, the molecules are decelerated. We will show the transport and deceleration of metastable CO molecules through an array formed by 63 deceleration stages. The oscillating motion of molecules in the travelling well is observed. By providing a minimum electric field on the molecular beam axis, molecules in low-field-seeking states are kept together in the transverse direction as well.

5.1.1. *Motion in the Stark decelerator*

Let us consider an array of electric field stages separated by a distance L, as shown in figure 7. Each stage consists of two parallel cylindrical metal rods with radius r, centred a distance $2r + d$ apart. One of the rods is connected to a positive and the other to a negative switchable high-voltage power supply. Alternating stages are connected to each other. When a molecule in a quantum state with a positive Stark effect (a low-field seeker) moves through the array of electric field stages as indicated in figure 7, it will gain Stark energy. This gain of potential energy is compensated by a loss of kinetic energy. If the electric field is abruptly switched off, the molecule will keep its instantaneous velocity. If, simultaneously, the electric field of the next stage is switched on, the process will repeat itself. In figure 7 the potential energy of the molecule, $W(z)$, is depicted as a function of its position z along the beam axis. The energy a molecule loses per stage depends on its position at the time that the fields are being switched. In analogy with concepts used in charged-particle accelerators, this position is expressed in terms of a 'phase angle' ϕ that has a periodicity of $2L$. Molecules that are in maximum electric field just prior to the time at which the fields are switched are assigned a phase angle $\phi = 90^\circ$.

First, we will discuss the situation where the electric fields are switched at equal time intervals, ΔT. Let us consider a molecule with a phase $\phi = 0^\circ$ and with a velocity that matches the frequency of the electric fields, i.e. a molecule that travels exactly the distance L in the time interval ΔT. This molecule will be referred to as the 'synchronous' molecule. Its phase and velocity are designated as the equilibrium phase ϕ_0 and the equilibrium velocity v_0 respectively. It is readily seen that (i) the phase and velocity of the synchronous molecule remain unchanged and (ii) that molecules with a slightly different phase or velocity will experience an automatic correction towards these equilibrium values. A molecule with a phase slightly larger than ϕ_0 and a velocity equal to v_0, for instance, will lose more energy per stage than

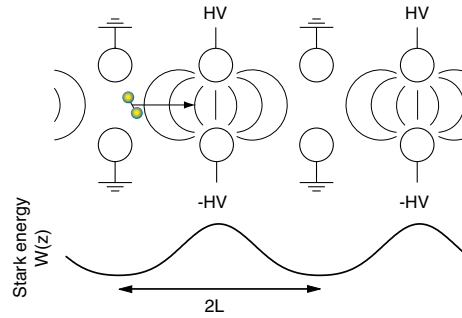

Figure 7. Scheme of the Stark decelerator, together with the Stark energy of a molecule as a function of position z along the molecular beam axis.

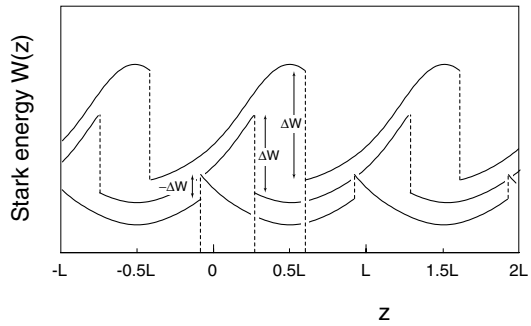

Figure 8. Potential energy for some molecules having the same velocity as the synchronous molecule ($v = L/\Delta T$). The phase of the different molecules $\phi = z'\pi/L$ with z' the position at the moment that the fields are being switched (dashed lines) is $-15°$, $45°$ and $105°$, for the lower, middle and upper curves respectively. The different curves have been given an offset for clarity.

the synchronous molecule. It will thus be slowed down relative to the synchronous molecule and consequently its phase will become smaller, until it lags behind. At this point, the situation is reversed and it will lose less energy than the synchronous molecule will, etc. This argument shows that molecules with a slightly different phase from ϕ_0 and/or a slightly different velocity from v_0 will oscillate with both phase and velocity around the equilibrium values; the molecules are trapped in a potential well travelling at the velocity of the synchronous molecule.

In order to decelerate the molecules one has to lower the velocity of the potential well, by gradually increasing the time intervals ΔT after which the electric fields are being switched. The synchronous molecule will still travel a distance L in the interval ΔT, but ϕ_0 will now be different from zero. By definition, the synchronous molecule is always at the same position when the fields are being switched (ϕ_0 remains constant); it will achieve this by losing exactly the required kinetic energy per stage. Again, the phase and velocity of a non-synchronous molecule will oscillate around those of the decelerated synchronous molecule.

In figure 8 the potential energy for three molecules is shown while they traverse the decelerator. The molecules have the same velocity as the synchronous molecule ($v = L/\Delta T$) but have a different position at the moment that the fields are being switched (a different phase). The different curves have been given an offset for clarity. It is seen that the energy the molecules lose or gain depends strongly on their phase.

The kinetic energy lost by the synchronous molecule per stage, $\Delta K(\phi_0)$, is given by $W(\phi_0) - W(\phi_0 + \pi)$. It is convenient to express $W(\phi)$ as a Fourier series. In the expression for $\Delta K(\phi_0)$ all the even terms cancel, yielding

$$\Delta K(\phi_0) = 2a_1 \sin(\phi_0) + 2a_3 \sin(3\phi_0) + \cdots. \tag{11}$$

When adjacent electric field stages are not too far apart, i.e. $L \sim 2r + d$, $\Delta K(\phi_0)$ is predominantly determined by the first term†. As mentioned above, the phase is only defined at the moment at which the fields are being switched. To be able to treat the motion of the molecules through the Stark decelerator mathematically, a

† Although convenient, the fact that the potential energy can be well represented by the first terms of the Fourier series of equation (11) does not have additional advantages.

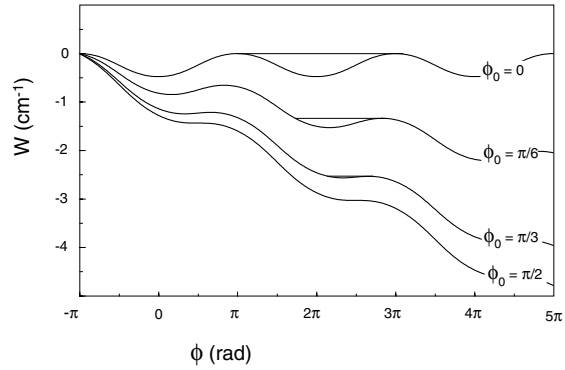

Figure 9. The potential energy for metastable CO molecules in the frame moving with the velocity of the synchronous molecule as a function of ϕ for four different values of ϕ_0. The potential energy is chosen to be zero at $\phi = -\pi$. The depth of the travelling potential well is equal to $0.48\,\mathrm{cm}^{-1}$ (680 mK), $0.19\,\mathrm{cm}^{-1}$ (270 mK), $0.03\,\mathrm{cm}^{-1}$ (43 mK) and $0\,\mathrm{cm}^{-1}$ (0 mK) for $\phi_0 = 0$, $\pi/6$, $\pi/3$ and $\pi/2$ respectively.

description in terms of continuous variables is needed. For a description of the motion of a non-synchronous molecule relative to the motion of the synchronous molecule, we will introduce the instantaneous difference in phase, $\Delta\phi = \phi - \phi_0$, and velocity, $\Delta v = v - v_0$. One can regard the lost kinetic energy per stage of the synchronous molecule as originating from a continuously acting average force, $\bar{F}(\phi_0) = -\Delta K(\phi_0)/L$. This approximation can be made provided that the deceleration rate, i.e. the amount by which the velocity of the synchronous molecule is reduced in a given stage relative to v_0, is small. When $\Delta v \ll v_0$, the average force on a non-synchronous molecule can be written as

$$\bar{F}(\phi_0 + \Delta\phi) \simeq -\Delta K(\phi_0 + \Delta\phi)/L. \tag{12}$$

We can calculate the travelling potential well by integrating equation (12) over ϕ. In figure 9 the potential well for metastable CO is shown for a number of values of ϕ_0 as used in our experiment (described below).

The equation describing the motion of the non-synchronous molecule relative to the motion of the synchronous molecule is given by

$$\frac{mL}{\pi}\frac{\mathrm{d}^2(\Delta\phi)}{\mathrm{d}t^2} + \frac{2a_1}{L}[\sin(\phi_0 + \Delta\phi) - \sin(\phi_0)] = 0, \tag{13}$$

with m the mass of the molecule. This is analogous to the equation of a pendulum driven by a constant torque. When $\Delta\phi$ is small, $\sin(\phi_0 + \Delta\phi) \simeq \sin\phi_0 + \Delta\phi\cos\phi_0$ and the equation of motion becomes

$$\frac{mL}{\pi}\frac{\mathrm{d}^2(\Delta\phi)}{\mathrm{d}t^2} + \frac{2a_1}{L}(\Delta\phi\cos\phi_0) = 0. \tag{14}$$

In figure 10 a numerical integration† of equation (13) is shown for various equilibrium phases ϕ_0. The full curves are lines of constant energy and indicate trajectories that molecules will follow. The inner curves are nearly elliptical, corresponding to a nearly linear restoring force on the molecules, as can be seen

† An analytical solution can also be found, see for instance Livingood (1961).

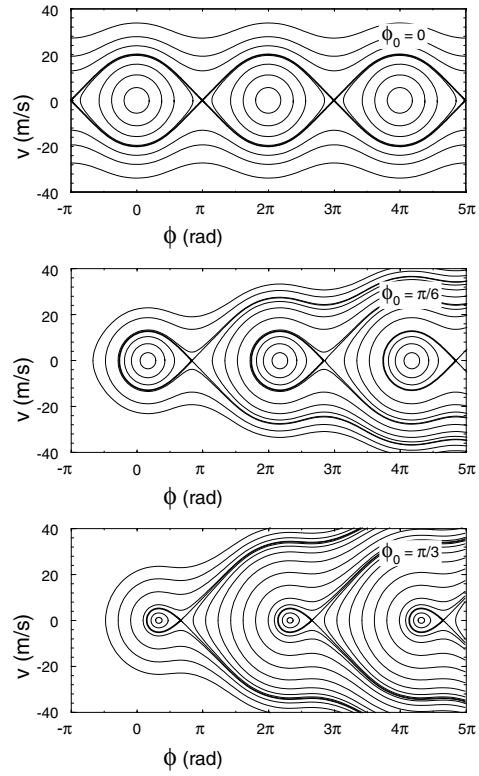

Figure 10. Phase stability diagrams for various values of ϕ_0, obtained via numerical integration of equation (13) with parameters as used in the experiment for metastable CO. In the experiment a difference in the phase angle of 2π corresponds to a distance of 11 mm.

from equation (14). For metastable CO the longitudinal oscillation frequency, given by

$$\frac{\omega_z}{2\pi} = \sqrt{\frac{a_1 \cos\phi_0}{2m\pi L^2}}, \tag{15}$$

is approximately 1 kHz for $\phi_0 = 60^\circ$. Further outward, the restoring force is less than linear and the oscillation frequency is lowered, approaching zero on the separatrix (thick curve). Beyond the separatrix the total energy of the molecules is larger than the effective potential well and the trajectories of the molecules are unbound. The area inside the separatrix ('bucket') is the longitudinal acceptance of the decelerator. It is seen that this area is larger for smaller values of ϕ_0. The deceleration per stage is given by equation (11) and increases when ϕ_0 is increased from 0 to $\frac{1}{2}\pi$. Since both a large acceptance and an efficient deceleration are desirable there is a trade-off between the two.

The phase stability diagrams showing the longitudinal acceptance of the Stark decelerator are very similar to those used to describe charged-particle accelerators (see, for instance, Edwards and Syphers (1993, figure 2.20)). There is an important difference, however. In a charged-particle accelerator energy is added to the particles at a certain position, while the amount of energy that is added depends on the time

they arrive at this position. In the Stark decelerator energy is added to the molecules at a certain time, while the amount of energy that is added depends on their position at that time. Therefore, while in charged-particle accelerators energy and time are conjugate variables, in the Stark decelerator this role is played by velocity (energy divided by velocity) and position (time multiplied by velocity). As a consequence, while the energy spread in the laboratory frame remains constant in a charged particle accelerator, the velocity spread in the laboratory frame remains constant in the Stark decelerator.

The description in phase space is very useful. Since in the model the time dependence is eliminated, the initial conditions of a molecule uniquely define its subsequent motion. Therefore, two trajectories can not cross in (two-dimensional) phase space; if they did, their position and velocity would be the same and they would have the same subsequent motion. This implies that a boundary which bounds a number of molecules at a certain time will transform into a boundary at a later time which bounds the same molecules. Therefore, we can follow the motion of a large group of molecules by following the motion of a much smaller group of boundary molecules (Lichtenberg 1969).

Phase stability ensures that the phase-space density remains constant during the deceleration process. In addition, it makes the deceleration insensitive to imperfections of the electric field in the decelerator, caused, for instance, by misalignments of the electrodes or fluctuations in the applied voltages. Small deviations from the expected electric field will make the phase ϕ_0, assumed to be constant throughout the decelerator, differ from stage to stage. This leads to a slightly modified acceptance area, with some blurring in the region of the separatrix. The final velocity, however, is determined by the time sequence only and is not altered.

Using the above derived relations we will now calculate the time sequence. From equation (11), the energy of the synchronous molecule as a function of its position in the decelerator is given by

$$E(z) = E(z=0) - \frac{z}{L} 2a_1 \sin\phi_0, \tag{16}$$

using only the first term in equation (11). The velocity of the synchronous molecule is thus given by

$$v(z) = \sqrt{v_z^2(z=0) - \frac{z}{L}\frac{2}{m} 2a_1 \sin\phi_0}. \tag{17}$$

We integrate this equation to find the time at which the synchronous molecule is in the nth stage,

$$t(n) = \int_0^{nL} \frac{\mathrm{d}z}{\sqrt{v_z^2(z=0) - (z/L)(2/m)2a_1 \sin\phi_0}}. \tag{18}$$

Also,

$$t(n) = L\left[v_z(z=0) - \sqrt{v_z^2(z=0) - n\frac{2}{m}2a_1 \sin\phi_0}\right] \Big/ \left(\frac{1}{m}2a_1 \sin\phi_0\right). \tag{19}$$

In figure 11 the time sequence for deceleration of metastable CO is shown using four different phases as indicated in the figure. The full curves show $\Delta T(n) = t(n+1) - t(n)$ calculated using equation (19). The crosses show the results of

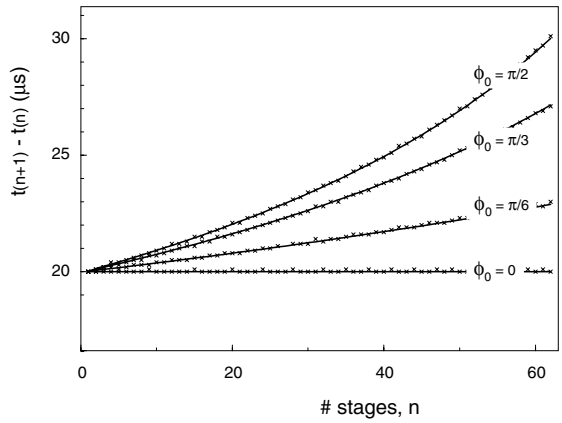

Figure 11. Time sequence for four different phases as indicated in the figure starting from a velocity of 275 m s^{-1}. The full curves show $\Delta T(n) = t(n+1) - t(n)$ calculated using equation (19), the crosses show the results of a numerical calculation.

numerical calculation using as input the electric field and the known Stark shift of metastable CO. The electric field is calculated using the finite-element program Simion 6.0 (Dahl 1995). Laplace's equation is evaluated on a $200 \times 88 \times 88$ grid (1 grid unit is 0.1 mm). Using the known Stark shift of metastable CO the potential energy and the acceleration are calculated on the same grid. The acceleration at any point is found by making a linear interpolation between the eight nearest grid points. The trajectory of a molecule through the array is found by numerically solving the equation of motion using a third-order Runge–Kutta procedure (Press *et al.* 1986). The switch times are calculated with a precision of 100 ns, which is the minimum timestep which can be entered in the delay generator (to be described later). For a phase angle of 60° metastable CO molecules are decelerated from 275 m s^{-1} to 200 m s^{-1} and the frequency of the electric fields is lowered from 50 kHz to 37 kHz.

By appropriately incorporating the time variation of the electric fields, the program that is used to calculate the time sequence numerically can also be used to calculate the trajectories of non-synchronous molecules through the array. In figure 12 the velocity of a number of metastable CO molecules is shown as a function of their position in the decelerator. The phase of the synchronous molecule is taken to be 60°. The initial position is taken to be the same for all molecules. As expected, one can observe a modulation with a period of L (= 5.5 mm). In the model this modulation is assumed to be small compared with the absolute value of the velocity or, at least, to have no net influence on the trajectory. The grey-shaded area shows the velocity interval for which stable phase oscillation occurs.

For the array of electrodes schematically depicted in figure 7, the electric field near the electrodes is higher than that on the molecular beam axis. Therefore, molecules in low-field-seeking states experience a force focusing them towards the molecular beam axis. This focusing occurs only in the plane perpendicular to the electrodes, i.e. in the plane of the figure. In order to focus the molecules in both transverse directions, the electrode pairs that make up one deceleration stage are alternately positioned horizontally and vertically.

In figure 13 the electric field in the decelerator is shown for two mutually perpendicular planes. Both planes that are shown have the molecular beam axis in

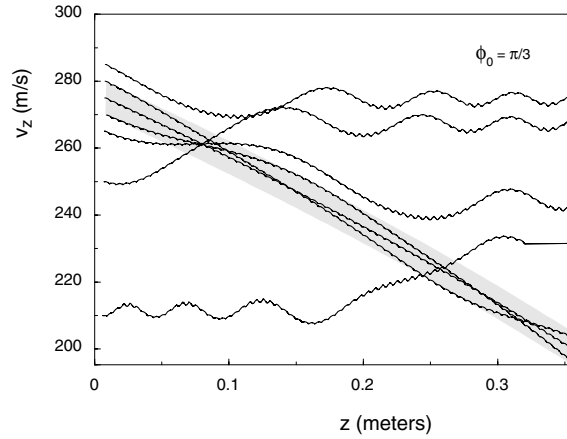

Figure 12. The velocity as a function of the position in the decelerator for a number of metastable CO molecules as obtained by numerically solving the equation of motion. The trajectories have been calculated using $\phi_0 = 60^\circ$. In this case the velocity of the travelling well is lowered from $275\,\mathrm{m\,s^{-1}}$ to $200\,\mathrm{m\,s^{-1}}$. The initial position is taken to be the same for all molecules. The grey-shaded area shows the velocity interval for which stable phase oscillation occurs.

common. The electric fields are calculated using a finite-element program, with parameters as in the experiment. The two opposing rods that make up one deceleration stage have a radius r of 1.5 mm and are spaced a distance d of 2 mm apart. Two adjacent deceleration stages are spaced a distance L of 5.5 mm apart. With a maximum voltage of $+10\,\mathrm{kV}$ and $-10\,\mathrm{kV}$ on the electrodes the maximum electric field on the molecular beam axis is $90\,\mathrm{kV\,cm^{-1}}$. Near the electrodes at high voltage the electric field is $120\,\mathrm{kV\,cm^{-1}}$. The electric fields shown in figure 13 are calculated for the situation with the electrodes along the x axis (front part) at ground potential and with the electrodes along the y axis (partly hidden) at high voltage. Therefore, molecules in low-field-seeking states are focused in the plane perpendicular to the electrodes at high voltage, as shown in the upper part of the figure. In the other direction the electric field is (nearly) constant and therefore there will be no focusing or defocusing in this direction. During the deceleration process the molecules pass through electric field stages that are alternately positioned horizontally and vertically and are therefore focused in either direction.

As can be seen from figure 13, the force experienced by a molecule depends on its position in the decelerator. In addition, it depends on the time sequence of the high-voltage pulses that are applied. A molecule is strongly focused when between the electrodes at high voltage but much less so further away from these electrodes. Therefore, the trajectories are generally complicated. When the focusing is not too strong, the z dependence of this force can be eliminated by introducing an average force. The transverse motion throughout the decelerator can then be described using this average force, which will now depend on the phase angle ϕ only. The motion of the molecules in the transverse potential well is characterized by a transverse angular oscillation frequency $\omega_t(\phi)$. The condition that the focusing is not too strong can be formulated as $2\pi/\omega_t \gg 2L/v_z$, i.e. that the time of transverse oscillation is much larger than the time it takes for the molecules to traverse one period (two stages) of the decelerator. Molecules with a longitudinal velocity close to the velocity of the

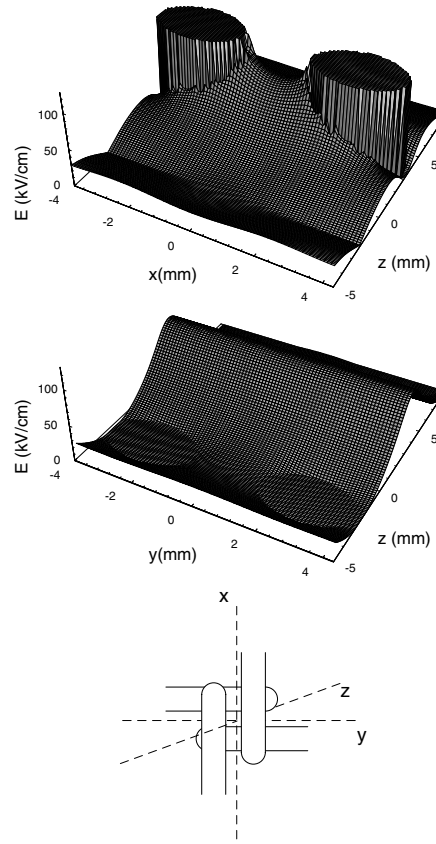

Figure 13. The electric field in two mutually perpendicular planes that have the molecular beam axis in common, together with a schematic view of two adjacent electric field stages. The two rods along the x axis are at ground potential, while the rods along the y axis are at $+10\,\mathrm{kV}$ and $-10\,\mathrm{kV}$. With these voltages the maximum electric field on the molecular beam axis is $90\,\mathrm{kV\,cm^{-1}}$. Near the electrodes at high voltage the electric field is $120\,\mathrm{kV\,cm^{-1}}$. (Figure reproduced from Bethlem *et al.* (2002b) with permission. Copyright the American Physical Society.)

synchronous molecules will traverse a distance L during ΔT, the time interval after which the voltages are being switched. The force needs to be averaged over $2L$:

$$\bar{F}_t(\phi) = \frac{1}{2L}\int_{\phi L/\pi}^{(\phi+2\pi)L/\pi} F_t(z)\,\mathrm{d}z. \tag{20}$$

Near the molecular beam axis, the average force is linearly dependent on the displacement from this axis. The full curve in figure 14 shows the resulting force constant ($1\,\mathrm{aN\,mm^{-1}} \simeq 0.05\,\mathrm{cm^{-1}\,mm^{-2}}$) for metastable CO. The broken curve shows the maximum depth of the transverse potential well, i.e. the depth 1 mm away from the molecular beam axis. Since the linear dependence of the force on the displacement holds rather well throughout, the curves are almost identical. For $\phi = 60^\circ$ the transverse well is $\sim 0.012\,\mathrm{cm^{-1}}$, or $\sim 17\,\mathrm{mK}$, deep. Molecules with a maximum transverse velocity of $3\,\mathrm{m\,s^{-1}}$ will, therefore, still be accepted in the

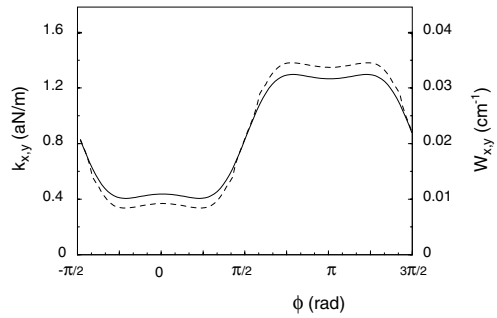

Figure 14. The average force constant (close to the molecular beam axis) for metastable CO as a function of ϕ (full curve) together with the maximum depth of the transverse potential well (broken curve), i.e. the depth 1 mm away from the molecular beam axis.

deceleration process. The frequency of transverse oscillation, $\omega_t/2\pi$, is approximately 700 Hz.

Generally a molecule oscillates between a minimum and a maximum phase and therefore experiences a different (average) transverse force along its path. The coupling between the longitudinal motion and the transverse motion may result in parametric amplification of the transverse oscillation. This effect might be expected to be strong, as the frequencies involved are rather similar. On the other hand, as the deceleration process only lasts 2–3 oscillation periods, parametric amplification is not expected to be important, as confirmed by numerical simulations. The maximum accepted transverse velocity is determined by the minimum depth of the transverse potential well through which the molecules pass. This implies that the maximum transverse acceptance is obtained for molecules with a phase around that of the synchronous molecule.

5.1.2. *Experimental set-up*

In order to demonstrate the performance of the Stark decelerator, experiments have been carried out on CO molecules in the $a^3\Pi$ state. The main reasons for using metastable CO molecules for these experiments are that (i) they can be prepared in a single quantum state at a well-defined position and time and (ii) their velocity distribution can be readily measured.

The experimental set-up, schematically depicted in figure 15, consists of a compact molecular beam machine, with two differentially pumped vacuum chambers. The source chamber and decelerator chamber are pumped by a 3001 s^{-1} and a 2401 s^{-1} turbo pump respectively. A pulsed beam of CO is formed by expanding a 5% CO in xenon mixture through a modified solenoid valve with a 0.8 mm diameter opening into vacuum. The solenoid valve (General Valves series 9) is modified such that it can be operated down to liquid nitrogen temperatures. In the CO experiments the valve housing is cooled to 180 K, just above the boiling point of Xe. The stagnation pressure is typically about 1.5 atm. The valve opens for a duration of 80 μs. The experiments run at 10 Hz, and under operating conditions the pressure in the source chamber and the decelerator chamber is typically 5×10^{-6} and 2×10^{-8} Torr respectively. The mean velocity of the CO molecules in the beam is 280 m s^{-1}, corresponding to an initial kinetic energy of $E_{\text{kin}} = 92\,\text{cm}^{-1}$. The velocity

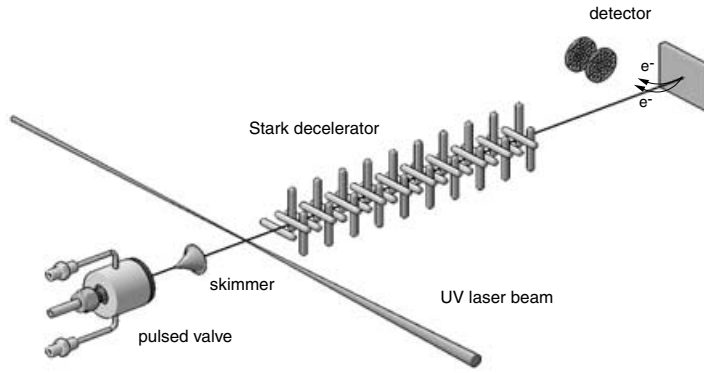

Figure 15. Scheme of the experimental set-up. State-selected metastable CO ($a^3\Pi_1$, $v' = 0$, $J' = 1$) molecules are prepared using pulsed-laser excitation of ground-state CO molecules. The beam of metastable CO molecules is slowed down on passage through a series of 63 pulsed electric field stages. The time-of-flight (TOF) distribution of the metastable CO molecules over the 54 cm distance from laser preparation to detection is measured via recording of the amount of electrons emitted from a gold surface when the metastable CO molecules impinge on it.

spread is approximately 12%, corresponding to a temperature of $0.48\,\mathrm{cm}^{-1}$ or $\sim 0.7\,\mathrm{K}$ in the moving frame. The CO molecules pass through a 1.0 mm diameter skimmer into a second differentially pumped vacuum chamber. Preparation of a pulsed beam of metastable CO molecules in single quantum levels is performed by direct laser excitation of the ground-state molecules via the spin-forbidden $a^3\Pi(v' = 0) \leftarrow X^1\Sigma^+(v' = 0)$ transition, using pulsed 206 nm (6.0 eV) radiation, as described in section 4.4. In our experimental set-up, the molecules need to be prepared in states that exhibit a positive Stark effect which are the upper components of the Λ doublets in the $a^3\Pi$ state. In the experiments reported here, laser preparation of the $J' = 1$ $a^3\Pi_1$ level via the $Q_2(1)$ transition is used. The laser is focused to a 0.3 mm diameter spot. At the intensities used, the spin-forbidden $a^3\Pi_1 \leftarrow X^1\Sigma^+$ transition can be fully saturated.

It is essential that the molecules remain in the low-field-seeking state throughout the decelerator. If the molecules entered a zero electric field, they might exit it in the $|J, M\Omega\rangle = |1, 0\rangle$ state, in which case they would be lost for the deceleration process. These Majorana transitions are avoided by ensuring that the electric field never drops below a certain minimum value (Harland *et al.* 1999). Furthermore, the rapid switching of the electric fields generates rf radiation that can induce transitions between Stark states. In order to avoid such transitions, the minimum electric field needs to be kept sufficiently high that the Stark splitting remains larger than the energy of the highest-frequency component of the rf radiation. Molecules moving through the decelerator never experience an electric field below $300\,\mathrm{V\,cm}^{-1}$, and no sign of a loss due to these transitions has been observed†.

The 35 cm long Stark decelerator consists of an array of 63 equidistant ($L = 5.5$ mm) electric field stages. Each deceleration stage is formed by two parallel

† It should be noted, however, that for molecules that have hyperfine structure, such as ND_3, the rapid switching of the electric fields can scramble the population between the various low-field-seeking hyperfine levels.

3 mm diameter cylindrical rods, spaced 2 mm apart. The rods are made from hardened steel and are highly polished. The two opposing rods are simultaneously switched by two independent high-voltage switches to a maximum of +15 kV and −15 V. All horizontal and vertical stages are electronically connected requiring a total of four independent high-voltage switches (Behlke Electronic GmbH, HTS-151-03-GSM). The switches are triggered by a programmable delay generator running at a clock frequency of 10 MHz. It is advantageous to operate the decelerator at the highest possible electric fields, since this will increase the acceptance of the decelerator. The maximum obtainable electric field strength is limited by field electron emission at the electrode surfaces. It is assumed that this will take place at field strengths over $\sim 10^4\,\mathrm{kV\,cm^{-1}}$ (Latham 1981), in principle allowing a voltage difference of 2000 kV over the 2 mm gap between the electrodes. In practice, however, electrical breakdown takes place at much lower voltage differences owing to field enhancement at microfeatures associated with the intrinsic microscopic roughness of the electrode surfaces. Breakdown events need not be disastrous as long as the energy that is dissipated in the gap is kept low. In fact, since discharges melt the surface locally, these events reduce the roughness of the surface, allowing the gap to withstand a higher voltage difference after the event. Since in the decelerator the electric fields are switched rapidly (within 200 ns), the resistance between the switches and the electrodes needs to be small (1 kΩ). Under these conditions it is likely that a discharge will permanently damage the surface, instead of improving it. Therefore, before operating the decelerator with time-varying electric fields, a constant electric field is used for high-voltage conditioning. The voltage difference is slowly increased while the current of the induced discharges is being limited. This procedure allows for an increase of the maximum attainable voltage difference between the electrodes without sparking. Typically, the voltage difference is increased by $5\,\mathrm{kV\,h^{-1}}$ while the current is limited to 1 μA. This procedure is repeated every time the decelerator has been exposed to air. After this treatment, the decelerator is operated at a voltage difference 25% below the maximum voltage difference sustainable during the high-voltage conditioning. In this way the decelerator could be operated routinely at +10 kV and −10 kV, corresponding to a maximum electric field of $120\,\mathrm{kV\,cm^{-1}}$ near the electrodes. It is believed that at present the maximum electric field is limited by currents running over the surface of the aluminum oxide rings that are used for suspension of the decelerator. By improving the mounting of the decelerator, it is expected that the electric fields could be increased to $200\,\mathrm{kV\,cm^{-1}}$ or more.

In all experiments presented here, the decelerator is operated at voltages of +10 kV and −10 kV. Under these conditions the maximum energy that can be lost in one stage for metastable CO is $0.8\,\mathrm{cm^{-1}}$ or 1.15 K. The velocity of the beam is determined by measuring the delay between excitation and the arrival of the molecules at the detector 54 cm downstream. The metastable CO molecules are detected by counting the number of electrons emitted from a flat gold surface when the metastable CO molecules impinge on it.

5.1.3. *Experimental results*

The actual number of electric field stages that is used can be varied by adjusting the computer-controlled sequence by which the switches are triggered. In the left part of figure 16 the measured TOF distributions are plotted for an increasing number of electric field stages used, as indicated in the figure. The experimental curves, which

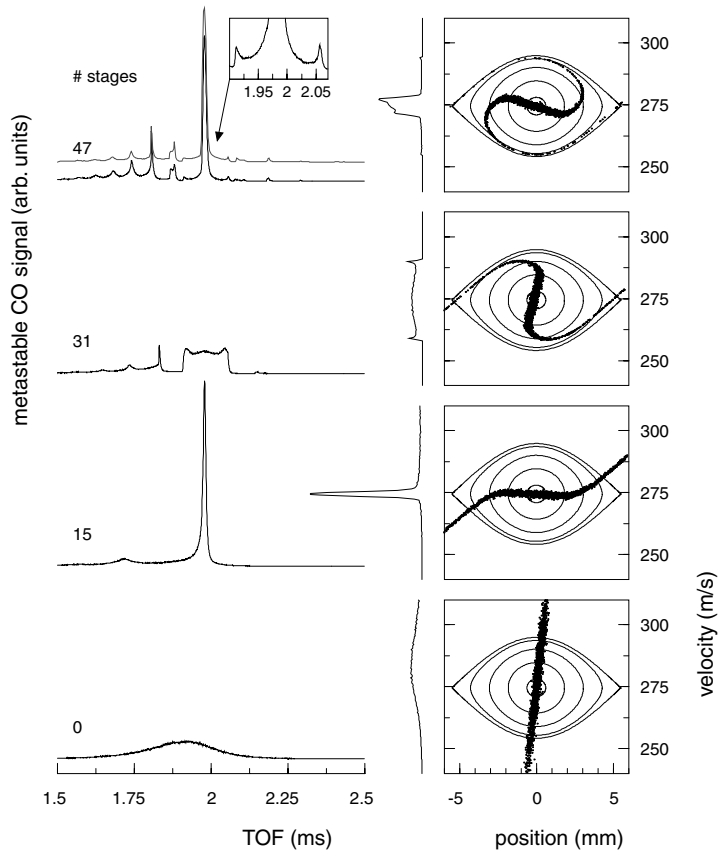

Figure 16. Observed TOF distributions using an increasing number of electrodes for $\phi_0 = 0°$. On the right, the results from a numerical simulation are plotted in phase-space diagrams, at the beginning of the decelerator and in the 15th, 31st and 47th stage. (Figure reproduced from Bethlem *et al.* 2000a) with permission. Copyright the American Physical Society.)

have been given an offset for clarity, are normalized to have the same integrated intensity; the actual intensity increases by more than a factor of 5 with increasing number of stages used owing to transverse focusing effects. The electric fields are switched at equal time intervals of $\Delta T = 20\,\mu s$, such that the travelling potential is moving at $275\,m\,s^{-1}$, close to the mean velocity of the molecular beam. By varying the number of electrodes used, the time that the trapping potential is on is varied. Therefore, the observed TOF distributions are snapshots of the motion of the metastable CO molecules in the travelling potential well. The width of the TOF distributions is a convolution of the spatial and velocity distributions of the trapped molecules. However, as the velocity spread of these molecules can be as large as 12% while the spatial extent of the bunch of molecules is always below 2% of the flight path, the TOF distribution mainly reflects the velocity distribution. The oscillation of the width of the TOF distributions with increasing number of stages and therefore directly reflects the oscillation in the velocity spread of the trapped molecules. The dotted curve above the TOF distribution recorded with 47 stages results from a numerical simulation of the trajectories through the decelerator. On

the right-hand side of figure 16, the results from the simulation for 0, 15, 31 and 47 electric field stages are plotted in phase-space diagrams together with several (including the outermost) orbits of the phase stability diagram for $\phi_0 = 0°$. The phase-space diagrams show the position and velocity of the molecules just after the travelling well is switched off. The position of a molecule in phase space is represented by a dot in these diagrams. The projections of the distributions of molecules in phase space on the velocity axis, as shown on the left axes, give the true velocity distributions of the trapped molecules. Since the metastable molecules are prepared in a 0.3 mm diameter laser focus, only a small region in phase space is occupied at the entrance of the Stark decelerator. This enables the direct observation of the oscillatory motion of the molecules in velocity and position. The molecules are seen to describe closed orbits in the position–velocity plane. Because of the anharmonicity of the travelling potential well the outer orbits have longer periods than the inner ones, resulting in spiral structures. The tails of these spirals are seen as sharp edges in the upper TOF distribution and are shown in more detail in the inset. The narrowest velocity distribution results when the distribution of the molecules in the phase-space diagrams is 'horizontal'. The ultimate width of the velocity distribution is determined by the initial spatial extent of the bunch of molecules at the entrance of the Stark decelerator. When 15 stages are used, the relative velocity spread is 0.7%, corresponding to a temperature in the moving frame of $T = 4\,\mathrm{mK}$.

The molecules trapped in the potential well can be decelerated by gradually increasing ΔT, at the cost of a decrease of the depth of the potential well. In figure 17 measured TOF distributions are plotted for an increasing number of electric field stages, using a time sequence calculated for $\phi_0 = 60°$. With these settings, the velocity of the travelling well is lowered from $275\,\mathrm{m\,s^{-1}}$ to $200\,\mathrm{m\,s^{-1}}$. The depth of the well is 43 mK; molecules with a full width at half-maximum velocity distribution of $4\,\mathrm{m\,s^{-1}}$ centred around the central velocity are captured. The molecules that have initial velocities outside this selected interval are, on average, not decelerated or accelerated. These molecules contribute to the more or less Gaussian distribution centred around the original arrival time in the TOF profiles. A hole can be observed where the decelerated bunch is sliced out. The intensity increases by more than a factor of 5 with an increasing number of stages used owing to transverse focusing effects.

For the upper curve, in which the maximum number of electric field stages is employed, the calculated TOF profile is shown as well (dotted curve), and is seen to describe the experimental observations well. Although not shown explicitly, all calculated TOF profiles are in good agreement with the observed ones, and both the observed intensity variations with the increasing number of electric field stages and the rather complicated structures that appear in the TOF profiles are well reproduced.

These measurements have been performed using a number of values for the phase of the synchronous molecule as shown in figure 18. All measurements are plotted on the same vertical scale. In figure 19 the experimentally observed fraction of the beam that is confined in the travelling potential well (right) is shown together with the kinetic energy loss of the metastable CO molecules over 47 stages (left) as a function of ϕ_0. The full curves shows the result using the analytical model with $2a_1 = 0.76\,\mathrm{cm^{-1}}$. Including the next term in the Fourier expansion with $2a_3 = -0.040\,\mathrm{cm^{-1}}$ yields the broken curves.

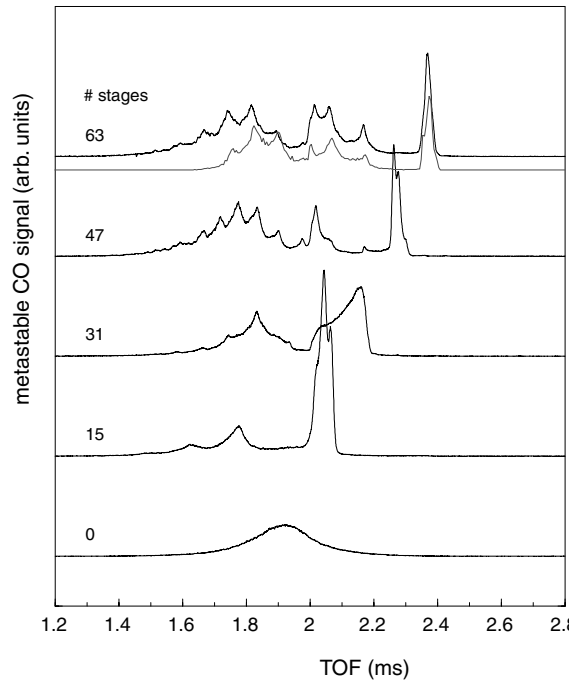

Figure 17. Observed TOF distributions using an increasing number of electrodes for $\phi_0 = 60°$. The measurements have been given an offset for clarity. The intensity is seen to increase by more than a factor of 5 with an increasing number of stages used owing to transverse focusing effects. The dotted curve shows a calculated TOF profile, to be compared with the upper of the measured curves.

One might conclude from figure 19 that the transverse focusing is largely independent of the phase of the synchronous molecule, in contrast to statements made in section 5.1.1. This, however, is a consequence of our experimental set-up. Our detector for metastable CO is found to have a rather small detection area. Furthermore, the molecules are decelerated using 47 stages, but the array consists out of 63 stages†. The last stages will act as a diaphragm. As a consequence these experiments are only sensitive to molecules with a rather small transverse velocity. The integrated intensity increases by a factor of $\sim$5 because in the decelerator the transverse spreading is 'frozen', thus increasing the number of molecules that arrive at the detector.

In order to decelerate metastable CO to a total standstill 90 stages are required. However, deuterated ammonia which has a slightly larger Stark shift and a smaller mass can be brought to a standstill in the existing decelerator. This is extensively discussed in Bethlem *et al.* (2002b).

The observed oscillation of the package of molecules while they traverse the decelerator is a consequence of the narrow initial position spread in our case. When using a molecule in its ground state the initial position spread (determined by the

† At 25 kHz the high-voltage switches are able to switch 47 times. When the frequency is lowered they are able to switch more often.

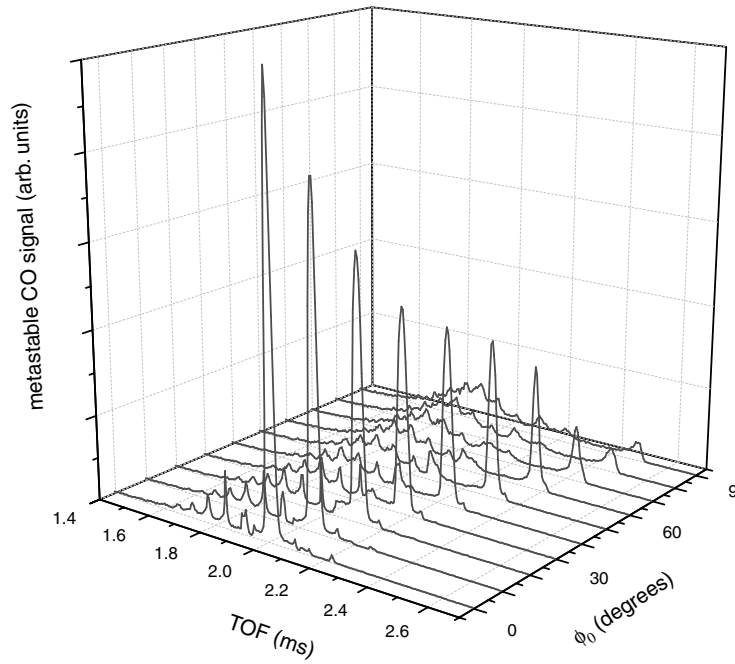

Figure 18. Observed TOF distributions using 47 electrodes for different values of ϕ_0. All measurements have the same vertical scale.

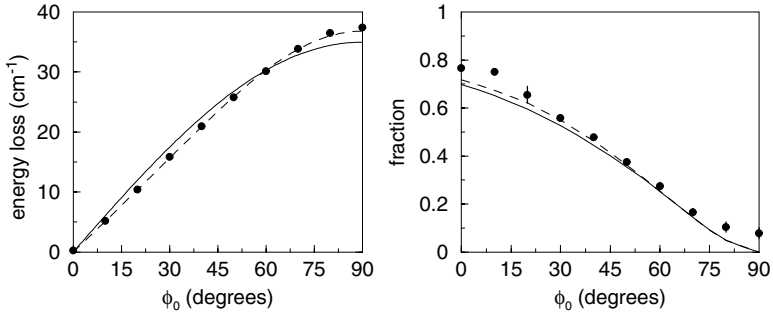

Figure 19. Observed kinetic energy loss over 47 stages (left) and the observed fraction of the molecular beam that is decelerated (right) as a function of ϕ_0, compared with results from the analytical model. (Figure reproduced from Bethlem *et al.* (2000a) with permission. Copyright the American Physical Society.)

pulsed valve) will be much larger than the acceptance of the decelerator. In this case the phase-space distribution of the decelerated package remains unaltered (see Bethlem *et al.* (2002b)). The shape of the phase-space distribution can be modified at will by using a second array mounted behind the decelerator operated at a phase angle of 0°. In Crompvoets *et al.* (2002) a package of ammonia molecules having a position spread of 1.1 mm and a velocity spread of 6.5 m s^{-1} (30 mK) is transformed into a package having a position spread of 10 mm and a velocity spread of 0.76 m s^{-1} (250 μK).

5.2. *Decelerating high-field seekers*

The rotational ground state of any molecule is always lowered in energy by an external perturbation, and is therefore a 'high-field-seeking' state. It would be a major advantage if molecules (and atoms (Maddi *et al.* 1999)) in this state could be decelerated as well. It might appear to be straightforward to apply the method presented in the previous sections also to molecules in high-field-seeking states by simply letting the molecules fly out of, instead of into, the region of a high electric field. For the motion of the molecules in the forward direction, this is indeed true. However, Maxwell's equations do not allow for a maximum of the electric field in free space (Wing 1984, Ketterle and Pritchard 1992), e.g. on the molecular beam axis, and therefore transverse stability cannot be maintained easily; molecules in high-field-seeking states have the tendency to crash into the electrodes, where the electric fields are the highest.

The same situation is encountered in charged particle accelerators where this problem has been resolved by applying the AG focusing method (Courant and Snyder 1958). This method came out of the realization that a long-established fact of geometrical optics was applicable to ion optics as well; for a pair of lenses that have equal focal lengths but with one lens converging and the other diverging, the total focal length is always positive. This same principle can be applied to polar molecules when using electrostatic dipole lenses. These lenses focus the molecular beam in one direction but simultaneously defocus the beam in the orthogonal direction. By alternating the orientation of these lenses, an electric field geometry with a focusing effect in both directions can be created. By switching these lenses on and off at the appropriate times, AG focusing and deceleration of a molecular beam can be achieved simultaneously.

5.2.1. *Transverse stability*

A scheme of the experimental setup used in Bethlem *et al.* (2002a) is shown in figure 20. The prototype AG decelerator consists of 12 dipole lenses, positioned symmetrically around the molecular beam axis. One of the lenses is shown enlarged in the inset at the left-hand side of figure 20, along with an $(\hat{x}, \hat{y}, \hat{z})$ axis system. A lens is composed of two identical thin electrodes (2 mm thick) with the side facing the molecular beam rounded off with a radius of curvature of 1 mm. The distance between the two electrodes is 2 mm. Typically, voltages of $+10$ kV and -10 kV are applied to these electrodes, yielding an electric field at the molecular beam axis close to 90 kV cm^{-1}. The electric fields along $\hat{x}$ and $\hat{y}$ are shown in the inset at the right-hand side of figure 20. It is seen that molecules in high-field-seeking states experience a force that repels them from the molecular beam axis in the plane of the electrodes and attracts them toward the molecular beam axis in the plane perpendicular to this. By symmetry, the defocusing force is equal to the focusing force close to the molecular beam axis. A molecule will alternately be focused and defocused while traversing the array of lenses. When the focal length of the lenses is well chosen, the displacement of a molecule from the molecular beam axis will be smaller at a negative lens than at a positive lens. Therefore, they will be more focused than defocused and their trajectories will be stable.

In figure 21 typical trajectories through the decelerator are shown using experimental parameters. The grey shaded area indicates the region of stable trajectories. It is seen that the beam envelope is larger at the positive lenses than at the negative lenses, as expected.

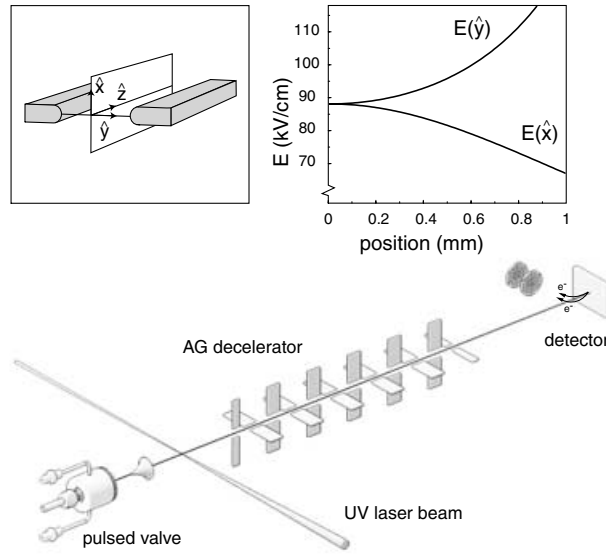

Figure 20. Scheme of the experimental set-up. State-selected metastable CO molecules are prepared using pulsed-laser excitation of ground-state CO molecules. The beam of metastable CO molecules is focused and decelerated using 12 electrodynamic dipole lenses in AG configuration. The TOF distribution of the metastable CO molecules over the 54 cm distance from laser preparation to detection is measured via recording of the number of electrons emitted from a gold surface when the metastable CO molecules impinge on it. In the inset at the left-hand side of the figure an enlarged view of a lens is shown together with an ($\hat{x}$, $\hat{y}$, $\hat{z}$) axis system. The electric fields along $\hat{x}$ and $\hat{y}$ are shown in the inset at the right-hand side of the figure. (Figure reproduced from Bethlem *et al.* (2002a) with permission. Copyright the American Physical Society.)

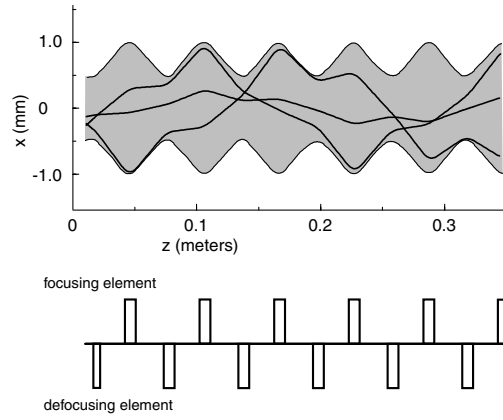

Figure 21. A number of trajectories through the AG decelerator. The grey-shaded area shows the beam envelope. (Figure reproduced from Bethlem *et al.* (2002a) with permission. Copyright the American Physical Society.)

5.2.2. *Alternate gradient deceleration*

In order to decelerate or accelerate the molecules, time-varying electric fields are applied. A molecule in a high-field-seeking state will gain kinetic energy as it enters the field of a lens, while it loses kinetic energy as it leaves the lens. When the electric field is switched on when the molecule is inside a lens, there will be no change to its kinetic energy but it will decelerate while leaving the lens. The moment when the field is switched on determines the effective length L of the lens; the focusing properties can thus be optimized without affecting the deceleration properties. Phase-stable operation can be obtained by switching the electric fields off again when the molecules have not yet left the field of a lens completely. In that case, molecules which are at the head of the pulse will lose more kinetic energy while molecules which are at the pulse's tail will lose less kinetic energy. Therefore, molecules in a narrow position and velocity interval will again be confined to this area of phase space throughout the decelerator.

5.2.3. *Experimental set-up*

In order to demonstrate the performance of the AG decelerator, experiments have been carried out on CO molecules in the $a^3\Pi$ state. For this experiment the molecules need to be prepared in states that experience a negative Stark shift which are the lower components of the Λ doublets in the $a^3\Pi$ state. In the experiments reported here, laser preparation of the $J' = 1\, a^3\Pi_1$ level via the $R_2(0)$ transition is used. By setting the polarization of the laser perpendicular to the stray fields present in the decelerator only the $M\Omega = 1$ high-field-seeking state is excited.

Laser preparation is performed in a 1 mm diameter spot, 5 mm in front of the 35 cm long AG decelerator consisting of an array of 12 equidistant 27 mm long dipole lenses. Successive lenses are separated by a 4 mm long drift region. The two opposing electrodes of a lens are simultaneously switched by two independent high voltage switches to maximum voltages of $+10$ kV and -10 kV. The first and last lenses have just half the length in order to have a more symmetric acceptance along $\hat{x}$ and $\hat{y}$. The TOF distributions over the 54 cm distance from laser preparation to detection are recorded by measuring the number of electrons emitted from a flat gold surface when the metastable CO molecules impinge on it.

5.2.4. *Experimental results*

In figure 22 the measured TOF distributions are plotted for several values of ϕ_0 as indicated in the figure. The lower curve is the TOF distribution of the original beam, when no voltages are applied, corresponding to a beam with a mean velocity of $275\,\mathrm{m\,s^{-1}}$. Using the 12 stages, molecules are decelerated from $275\,\mathrm{m\,s^{-1}}$ to $260\,\mathrm{m\,s^{-1}}$, or accelerated from $275\,\mathrm{m\,s^{-1}}$ up to $289\,\mathrm{m\,s^{-1}}$, depending on the phase angle ϕ_0 that is used. The thin curves show the results of a numerical simulation. The calculations are seen to describe the TOF distributions for the decelerated bunch rather well; a similarly good agreement is obtained in the simulation for the accelerated beam (not shown). In order to match the measured TOF distributions we have scaled down the simulations by a factor of 20; on applying the electric fields the integrated signal decreases by a factor of ~ 7 where we would have expected an increase in signal by at least a factor 3. This discrepancy is most likely to be due to misalignments in the decelerator; with a random displacement of ± 0.2 mm of the lenses the observed TOF distributions can be quantitatively reproduced.

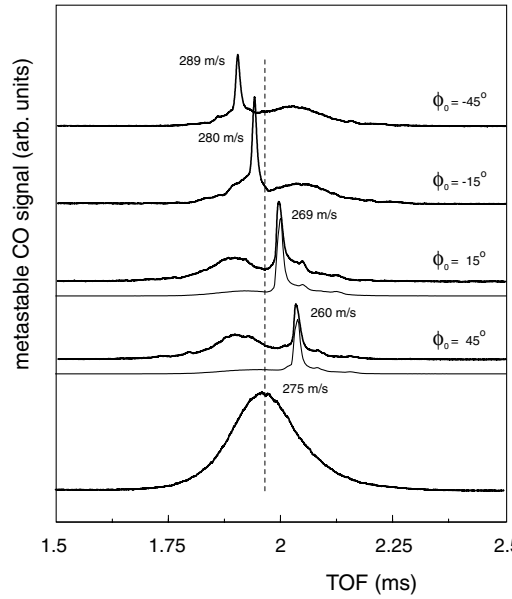

Figure 22. Observed TOF distributions of metastable CO over the 54 cm path length through the apparatus for four different phases as indicated in the figure, together with the TOF distribution when no electric fields are applied (lower curve). The measurements (thick curves) have been given an offset for clarity. The thin curves show the results of a numerical simulation. The broken line shows the expected arrival time of a molecule flying with a (constant) velocity of $275\,\mathrm{m\,s^{-1}}$. (Figure reproduced from Bethlem *et al.* (2002a) with permission. Copyright the American Physical Society.)

The proof-of-principle experiment demonstrates the potential of an AG decelerator for producing beams of polar molecules with arbitrarily (low) velocities. In the deceleration process the phase-space density remains constant; bunches of molecules are kept together independent of the number of lenses used in the decelerator. With the present geometry, 90 lenses would be required to bring the metastable CO molecules to a standstill. For this, the mechanical design of the decelerator must be improved. Alternatively, a geometry where a single lens is composed of multiple deceleration stages can be used, i.e. a geometry with a number of subsequent electrode pairs oriented along the same plane. The latter design is expected to be less susceptible to misalignment. Although more difficult to implement, AG deceleration can be used for both low-field- and high-field-seeking states.

6. Storing and trapping

The molecular beams with variable forward velocity (and thus variable de Broglie wavelength) and velocity spread as presented in the previous section offer fascinating perspectives for molecule optics, molecular collision studies, reactive scattering and surface science experiments. Performing crossed-beam experiments with two Stark-decelerated beams, for instance, would make it possible to measure cross-sections as a function of the centre-of-mass energy. One of the more obvious applications of the slow molecular beam is to use it to load traps and storage rings.

6.1. *A hexapole storage ring for polar molecules*

Multipole focusers can be regarded as two-dimensional traps. By bending a multipole focuser into a torus, molecules can be trapped in three dimensions (Katz 1997). This storage ring can be considered to be the electrostatic analogue of the magnetic bottle as used by Paul and coworkers to store neutrons (Kügler *et al.* 1978). The maximum velocity that the molecules can have in the torus is proportional to the square root of the torus's radius. In figure 23 the set-up is shown as used in Crompvoets *et al.* (2001). In the inset the effective potential energy is shown for ammonia molecules flying with a forward velocity of 89 m s^{-1}. As can be seen there is a position slightly off centre where the centrifugal force is balanced by the electrostatic force. Molecules in low-field-seeking states will experience a force towards this position. For the parameters used, molecules with a transverse velocity

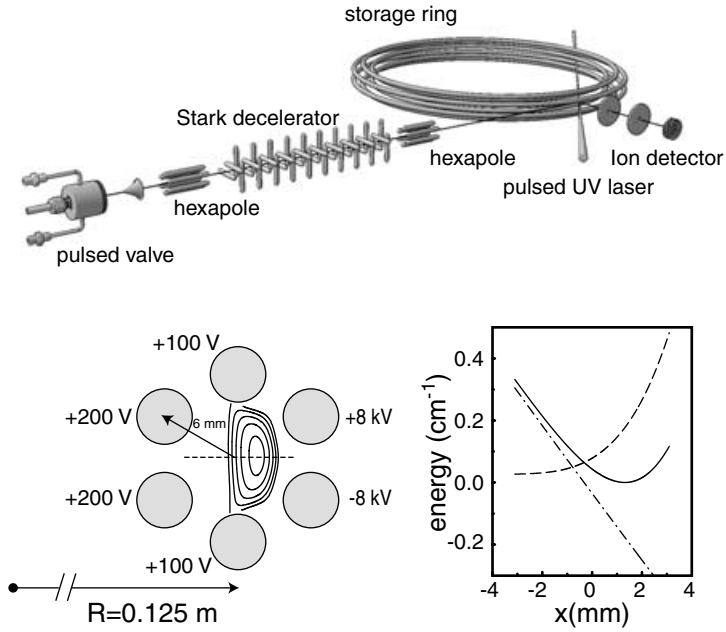

Figure 23. Experimental set-up. Upper part, from left to right: a gas pulse of less than 1% ND_3 in Xe exits a cooled ($T = 200$ K) pulsed valve with a mean velocity of 275 m s^{-1}. The beam is focused into the decelerator and slowed down to 89 m s^{-1}. The bunch of slow molecules is tangentially injected into the electrostatic storage ring (12.5 cm radius; 4 mm diameter rods). Molecules in the detection region of the storage ring are ionized using a pulsed laser, after which they are extracted and detected with an ion detector. In the lower part (left) the cross-section of the hexapole storage ring is shown with contour lines of equal potential energy at 0.02 cm^{-1} intervals for ND_3 molecules in the $|JK\rangle = |11\rangle$ state with positive Stark shift and with a tangential velocity of 89 m s^{-1}. In the right side of the inset the Stark energy (broken curve) is shown as a function of the displacement from the centre of the hexapole (x) in the plane of the hexapole ring (along the broken axis as shown in the left part of the figure). The full curve is obtained by adding the potential energy as a result of the centrifugal force for an ammonia molecule with a tangential velocity of 89 m s^{-1} (chain curve) to the Stark energy. The minimum of the resulting potential well is located 1.3 mm offset from the geometrical centre of the hexapole. (Reprinted by permission from *Nature* (Crompvoets *et al.* 2001). Copyright (2001) MacMillan Publishers Ltd.)

of up to $5\,\mathrm{m\,s^{-1}}$ will be confined in the ring. From the potential energy curve the ratio between the (transverse) position and velocity spread can be found. If a package of molecules is injected with a different aspect ratio, i.e. if the shape of the package of molecules in phase space does not match the acceptance of the ring, the molecules will start to oscillate. This will result in a loss in phase-space density. Therefore a hexapole is placed between the decelerator and the storage ring and serves as a lens which images the phase-space area of the package of molecules at the exit of the decelerator onto the ring. The magnification of the image is determined by the ratio between the distance from the decelerator to the hexapole and the distance from the hexapole to the ring.

The ammonia molecules are detected by resonantly ionizing them using a pulsed UV laser and counting the resulting ions. The package of slow molecules is observed to make up to six roundtrips. Because of their velocity spread (corresponding to 10 mK) the bunches of molecules gradually spread out along the ring. In order to compensate for this, the ring should be opened and a buncher, similar to the one used in Crompvoets *et al*. (2002), inserted. A sectional version of the storage ring will allow field-free interaction regions and various out-coupling regions. In such a ring, bunches of cold molecules can be made to interact repeatedly, at well-defined times and at distinct locations, with electromagnetic fields and/or particles. This yields unique opportunities for high-resolution spectroscopy and very sensitive collision studies.

A hexapole bend into a circle forms a trap for molecules in low-field-seeking states. Similarly, an AG focuser could be bent into a circle (Auerbach *et al*. 1966) by which molecules in both high- and low-field-seeking states can be trapped. Alternatively, a ring could be constructed out of separate bending and focusing fields, similar to a storage ring for charged particles. The bending elements could be similar to the wedge shown in figure 2; an AG lens pair could then be used to focus the molecules in the transverse and, by using time-varying electric fields, in the forward direction (Gould 2000). Molecules in high-field-seeking states can also be trapped using a coaxial focuser with an appropriately shaped outer electrode (Sekatskiĭ 1995, Sekatskiĭ and Schmiedmayer 1996, Jongma *et al*. 1997a, Loesch and Scheel 2000). These traps rely on the fact that molecules have a non-zero forward velocity to maintain stability. Molecules can also be trapped at a static point. Since Maxwell's equations allow for a minimum but not for a maximum of the electric field in free space (Wing 1984, Ketterle and Pritchard 1992), only molecules in low-field-seeking states can be trapped in a static trap. It is proposed, however, that molecules in high-field-seeking states may be trapped in an AC electric trap (Shimizu and Morinaga 1992, Peik 1999). This trap may be viewed as an AG focuser whose fields are switched to act alternately horizontally and vertically while the molecules stay at the same position. AC magnetic traps have been demonstrated for neutral atoms (Lovelace *et al*. 1985, Cornell *et al*. 1991); however, these traps suffer from heat produced in the trap coils. This problem is absent for electrodynamic traps. Trapping polar molecules in high-field-seeking states might be crucial for the success of evaporative cooling (Bohn, 2001).

6.2. *A quadrupole trap for polar molecules*

Wing proposed an electrostatic trap consisting of a ring electrode with two endcaps (Wing 1980). This trap may be viewed as a quadrupole torus with a radius equal to zero. The geometry of the trap is the same as that of a Paul trap for charged

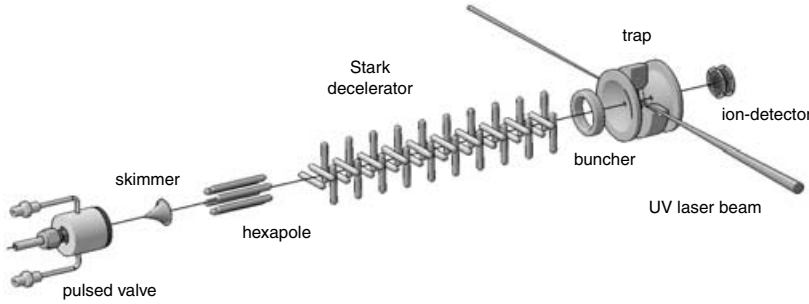

Figure 24. Schematic view of the experimental set-up. From left to right: a gas pulse of less than 1% ND_3 in Xe exits a cooled ($T = 200\,K$) pulsed valve with a mean velocity of $275\,m\,s^{-1}$. The beam is focused into the decelerator and slowed down to $15\,m\,s^{-1}$. Using a ring electrode the molecules are focused (in all three directions) into a quadrupole trap. In order to detect the ammonia molecules a pulsed laser is focused inside the trap. The resulting ions are extracted and counted using an ion detector. (Figure reproduced from Bethlem *et al.* (2002b) with permission. Copyright the American Physical Society.)

particles (Paul 1990). However, instead of rf fields, static electric fields are used for trapping neutral molecules. The inner radius R of the ring electrode is 5 mm. The endcaps are spaced $\sqrt{2}R$ apart. In the endcaps 2 mm diameter holes are made to enable the molecular beam to pass through. In the ring electrode 2 mm diameter holes are made to allow for laser detection of the trapped molecules at the centre of the trap. The electric field at the centre of the quadrupole is zero and increases linearly with distance from the centre†. In weak electric fields the Stark shift of ammonia is quadratic and the restoring force close to the centre is then linear in the displacement. In higher electric fields the Stark shift becomes linear and the force becomes constant. With a voltage difference of 12 kV between the ring electrode and the endcaps the trap depth for ND_3 is about $0.24\,cm^{-1}$, or 350 mK. The maximum velocity of $^{14}ND_3$ molecules which can be confined in the trap with these settings is approximately $17\,m\,s^{-1}$.

The experimental set-up used for trapping is schematically depicted in figure 24 (Bethlem *et al.* 2000b, 2002b). To load the trap, a beam of ammonia molecules is decelerated to $15\,m\,s^{-1}$. In order to bring the average velocity of the beam down to zero, the voltages are initially applied asymmetrically to the trap electrodes. With a voltage of 10 kV on the entrance endcap and 12 kV on the ring electrode, the electric field is small at the entrance of the trap and increases towards the centre of the trap. The synchronous molecule comes to a standstill at the centre of the trap. As before, it is necessary to match the emittance of the decelerated beam onto the acceptance of the trap. In this case, the beam must also be focused in the longitudinal direction. This is done with a ring electrode which is mounted in front of the entrance endcap of the trap. By applying a voltage difference between this ring electrode and the entrance endcap, an electric field is generated with a minimum on the molecular beam axis, focusing molecules in low-field-seeking states in the transverse directions.

† It is also possible to devise traps having an electric field minimum which is different from zero (Xu 2001), which may be important to prevent possible Majorana transitions at the centre of the trap.

Unlike in a hexapole, this minimum electric field is non-zero. This non-zero field on the molecular beam axis can be used to focus the molecules in the longitudinal direction ('bunching'). In this way a 6D area in phase space is imaged from the source region of the molecular beam onto the trap.

To detect the molecules the high voltages are switched off and a laser beam is focused inside the trap. Using a pulsed tunable UV laser the ammonia molecules are ionized in a $(2 + 1)$ resonance-enhanced multiphoton ionization (REMPI) scheme. Mass-selective detection of the parent ions is performed using the trap electrodes as extraction electrodes in a Wiley–McLaren type mass spectrometer set-up, as shown in figure 25. For this, a voltage of -300 V is applied to the exit endcap. The field-free flight tube is kept at -1.2 kV and the ion signal is recorded using a microchannel plate (MCP) detector placed further downstream. In the lower part of figure 25 a typical mass spectrum is shown with the laser frequency resonant on either $^{14}ND_3$ (upper curve) or $^{15}ND_3$ (lower curve). The ion signal is proportional to the density of neutral ammonia molecules at the centre of the trap.

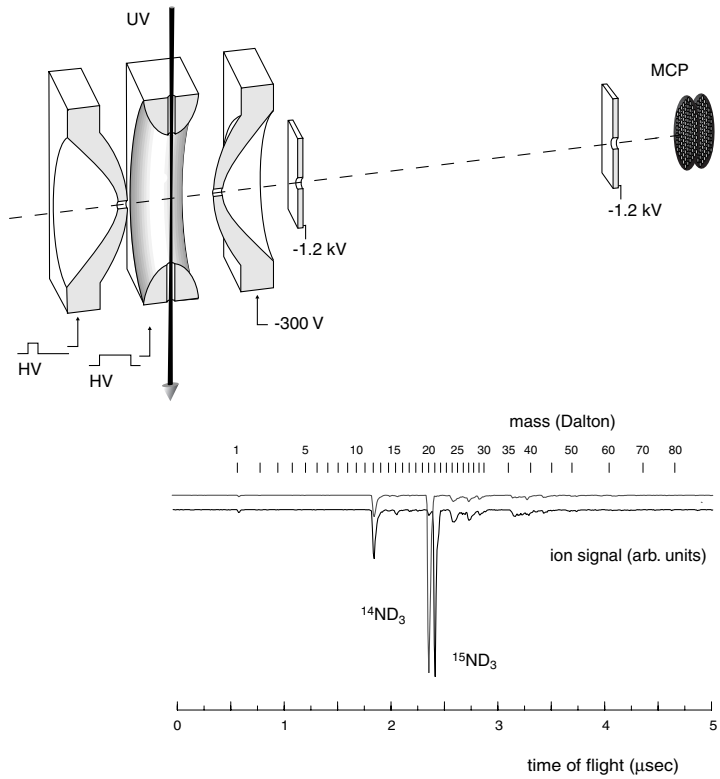

Figure 25. Schematic view of the trap. The ammonia molecules are detected by resonantly ionizing them using a tunable UV laser. The produced ions are extracted and detected on an MCP detector. In the lower part of the figure a typical mass spectrum recorded in the trap is shown. The measurements are taken while $^{14}ND_3$ and $^{15}ND_3$ are simultaneously trapped. The upper and lower curves are recorded when the laser radiation is resonant with a transition in $^{14}ND_3$ and $^{15}ND_3$ respectively. The peaks around 12, 24 and 36 Da are due to fragmentation of oil in the laser focus.

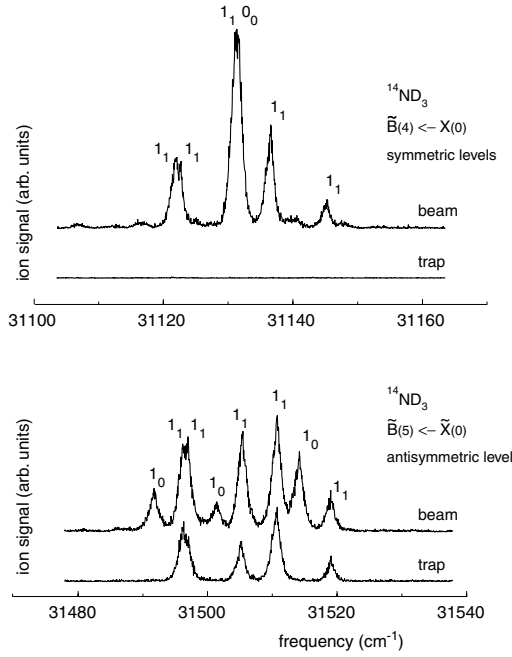

Figure 26. $(2+1)$-REMPI spectra recorded via the $\tilde{\mathbf{B}}\ ^1\mathrm{E}''$, $\nu_2' = 4$ (upper panel) and $\nu_2' = 5$ (lower panel) state in $^{14}ND_3$. In each panel, the upper curves are from measurements on the molecular beam, whereas the lower curves are recorded on the trapped molecules. (Figure reproduced from Bethlem *et al.* (2002b) with permission. Copyright the American Physical Society.)

In figure 26, $(2+1)$-REMPI spectra of $^{14}ND_3$ are shown, recorded via intermediate states of different vibrational symmetry. The spectra are recorded under conditions close to saturation, and the width of the lines is determined by power broadening. All spectra are shown with the same intensity scale and are averaged over 40 shots. In the upper panel, the $\nu_2' = 4$ vibrational level in the $\tilde{\mathbf{B}}^1\mathrm{E}''$ state is used as intermediate. Via this level, only molecules in the lower inversion doublet levels of ammonia are detected. Measurements are shown for the molecular beam (upper trace) and for trapped molecules (lower trace), both recorded using the trap as TOF mass spectrometer. The J_K rotational quantum numbers of the ground-state levels are indicated in the figure (Ashfold *et al.* 1988). In the lower panel, the $\nu_2' = 5$ vibrational level is used as intermediate, allowing only detection of molecules in the upper inversion doublet levels (vibrational *a* symmetry).

In the beam, both *s* and *a* components of the 0_0 and 1_0 ortho levels and the 1_1 para level are observed. The 1_0 and 1_1 levels are located $10\,\mathrm{cm}^{-1}$ and $8\,\mathrm{cm}^{-1}$ above the rotational ground-state level respectively. This implies a rotational temperature well below 3 K. The spectra of the trapped molecules show only the five allowed transitions originating from the upper inversion doublet level of the 1_1 state, which is the only populated low-field-seeking state in the beam. The density in the trap is roughly two times smaller than in the beam.

In order to determine the temperature of the trapped ammonia molecules, the spatial distribution of the molecules in the trap was measured along the *z* axis. This is done by scanning the position of the focused detection laser through the 2 mm

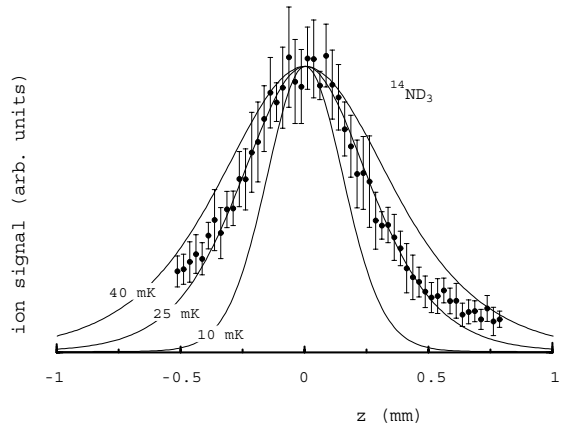

Figure 27. Density of trapped $^{14}ND_3$ molecules recorded as a function of the position along the z axis. The full curves show the results of a numerical simulation for thermal distributions with different temperatures. (Figure reproduced from Bethlem *et al.* (2002b) with permission. Copyright the American Physical Society.)

diameter holes in the ring electrode of the trap. The detection laser is fired after the molecules have been trapped for 50 ms, long compared with the oscillation periods in the trap. Since the density in the trap is low, no collisions between trapped molecules take place during this time interval. Strictly speaking, temperature is not defined in this case; it is used here as a measure of the average energy of the molecules in the trap. Knowing the trapping potential for $^{14}ND_3$ molecules in the $|J, K\rangle = |1, 1\rangle$ low-field-seeking state, the spatial and velocity distribution can be calculated assuming a certain temperature (Luiten *et al.* 1996).

In figure 27 the density of trapped $^{14}ND_3$ molecules is shown as a function of the position along the z axis. The detection efficiency is constant over the range in z covered in these measurements. Each data point is averaged over 10 trapping cycles. The error bars indicate the statistical spread in the measurements. The full curves are the results of a numerical simulation, assuming a thermal distribution of molecules in the trapping potential. The measurements are best described using a thermal distribution with a temperature of 25 mK. The density of the trapped molecules is estimated to be 1.3×10^7 molecules cm^{-3}. The total number of molecules is then 10^4. The phase-space density is 2×10^{-13}, roughly 50 times lower than the phase-space density in the beam. This loss is attributed to the not yet ideal loading of the trap.

Identical measurements have been performed on $^{15}ND_3$ using the same time sequence as in the experiment on $^{14}ND_3$. Within the experimental accuracy the measured density is the same for both isotopomers of ammonia. Both isotopomers have also been trapped simultaneously at a factor of 2 lower peak density for each species.

If only a single pulse is trapped, the phase-space density in the trap is ultimately limited by the phase-space density that can be obtained in the beam. In a pulsed supersonic expansion, densities of 10^{13} molecules cm^{-3} at a translational temperature of 1 K are routinely obtained (Miller 1988), implying a phase-space density of 10^{-9} and higher. For our beam we would expect a phase-space density on the order of 2.5×10^{-9} (see section 3.2.3). The measured phase-space density in our beam is much less. This might be due to insufficient pumping capacity in the current set-up or

excessive cluster formation. It might also indicate that we overestimate our detection efficiency.

7. Conclusions

The field of cold molecules is a rapidly growing field of research. While virtually non-existent 5 years ago, at the moment (August 2002) some 20 experimental groups and a dozen of theoretical groups are working on cold molecules. Several experimental methods to produce samples of translationally cold molecules have been successfully demonstrated over the last few years and a number of other schemes have been proposed. These methods are largely complementary. Photoassociation can be applied to homonuclear alkali and alkaline molecules as well as on H_2. Buffer-gas cooling can be applied to paramagnetic molecules and Stark deceleration is suited for dipolar molecules. Highly polarizable molecules such as I_2 could be decelerated using a moving optical lattice. All methods have their specific problems which need to be taken care off before useful densities of ultracold molecules are available. However, the rewards certainly seem to make the efforts worthwhile.

Acknowledgements

Many colleagues in Nijmegen and Nieuwegein have contributed to the work described in this review, in particular Giel Berden, Floris Crompvoets, Rienk Jongma, Bas van de Meerakker, Allard Mosk, André van Roij, Boris Sartakov, Paul Smeets, Chris Timmer, Jacqueline van Veldhoven and Michael Ziskind. Helpful discussions with Mike Tarbutt, Ed Hinds and Bretislav Friedrich are acknowledged. This work is part of the research programme of the Stichting voor Fundamenteel Onderzoek der Materie (FOM), which is financially supported by the Nederlandse Organisatie voor Wetenschappelijk Onderzoek (NWO).

References

Abraham, E. R. I., McAlexander, W. I., Sackett, C. A., and Hulet, R. G., 1995, Spectroscopic determination of the s-wave scattering length of lithium. *Phys. Rev. Lett.*, **74**, 1315.

Anderson, M. H., Ensher, J. R., Matthews, M. R., Wieman, C. E., and Cornell, E. A., 1995, Observation of Bose–Einstein condensation in a dilute atomic vapor. *Science*, **269**, 198.

Ashfold, M. N. R., Dixon, R. N., Little, N., Stickland, R. J., and Western, C. M., 1988, The $\tilde{B}^1E''$ state of ammonia: sub-Doppler spectroscopy at vacuum ultraviolet energies. *J. chem. Phys.*, **89**, 1754.

Auerbach, D., Bromberg, E. E. A., and Wharton, L., 1966, Alternate-gradient focusing of molecular beams. *J. chem. Phys.*, **45**, 2160.

Bahns, J. T., Stwalley, W., and Gould, P. L., 2000, Formation of ultracold molecules ($T \leqslant 1\,\mathrm{K}$) via photoassociation in a gas of laser-cooled atoms. *Adv. atomic mol. opt. Phys.*, **42**, 171.

Balakrishnan, N., and Dalgarno, A., 2001, Chemistry at ultracold temperatures. *Chem. Phys. Lett.*, **341**, 652.

Balakrishnan, N., Dalgarno, A., and Forrey, R. C., 2000, Vibrational relaxation of CO by collisions with ^{4}He at ultracold temperatures. *J. chem. Phys.*, **113**, 621.

Baranov, M. A., Mar'enko, M. S., Rychkov, V. S., and Shlyapnikov, G. V., 2002a, Superfluid pairing in a polarized dipolar Fermi gas. *Phys. Rev.* A, **66**, 013606.

Baranov, M., Dobrek, L., Góral, K., Santos, L., and Lewenstein, M., 2002b, Ultracold dipolar gases–a challenge for experiments and theory. cond-mat/0201100.

Barker, P. F., and Shneider, M. N., 2001, Optical microlinear accelerator for molecules and atoms. *Phys. Rev.* A, **64**, 033408.

Baugh, D. A., Young Kim, D., Cho, V. A., Pipes, L. C., Petteway, J. C., and Fuglesang, C. D., 1994, Production of a pure, single ro-vibrational quantum-state molecular beam. *Chem. Phys. Lett.*, **219**, 207.

Bennewitz, H. G., Paul, W., and Schlier, C., 1955, Fokussierung polarer Moleküle. *Z. Phys.*, **141**, 6.

Bethlem, H. L., Berden, G., and Meijer, G., 1999, Decelerating neutral dipolar molecules. *Phys. Rev. Lett.*, **83**, 1558.

Bethlem, H. L., Berden, G., van Roij, A. J. A., Crompvoets, F. M. H., and Meijer, G., 2000a, Trapping neutral molecules in a traveling potential well. *Phys. Rev. Lett.*, **84**, 5744.

Bethlem, H. L., Berden, G., Crompvoets, F. M. H., Jongma, R. T., van Roij, A. J. A., and Meijer, G., 2000b, Electrostatic trapping of ammonia molecules. *Nature (London)*, **406**, 491.

Bethlem, H. L., van Roij, A. J. A., Jongma, R. T., and Meijer, G., 2002a, Alternate gradient focusing and deceleration of a molecular beam. *Phys. Rev. Lett.*, **88**, 133003.

Bethlem, H. L., Crompvoets, F. M. H., Jongma, R. T., van de Meerakker, S. Y. T., and Meijer, G., 2002b, Deceleration and trapping of ammonia using time-varying electric fields. *Phys. Rev.* A, **65**, 053416.

Bohn, J. L., 2001, Inelastic collisions of ultracold polar molecules. *Phys. Rev.* A, **63**, 052714.

Bromberg, E. E. A., 1972, Acceleration and alternate-gradient focusing of neutral polar diatomic molecules. PhD thesis, University of Chicago.

Bulthuis, J., Möller, J., and Loesch, H. J., 1997, Brute force orientation of asymmetric top molecules. *J. phys. Chem.* A, **101**, 7684.

Chien, K.-R., Foreman, P. B., Castleton, K. H., and Kukolich, S. G., 1974, Relaxation cross section measurements on NH_3 and lower state focussing in a beam maser. *Chem. Phys.*, **7**, 161.

Chu, S., 1998, Nobel lecture: The manipulation of neutral particles. *Rev. mod. Phys.*, **70**, 685.

Cohen-Tannoudji, C. N., 1998, Nobel lecture: manipulating atoms with photons. *Rev. mod. Phys.*, **70**, 707.

Corkum, P. B., Ellert, C., Mehendale, M., Dietrich, P., Hankin, S., Aseyev, S., Rayner, D., and Villeneuve, D., 1999, Molecular science with strong laser fields. *Faraday Discuss.*, **113**, 47.

Cornell, E. A., Monroe, C., and Wieman, C. E., 1991, *Phys. Rev. Lett.*, **67**, 2439.

Courant, E. D., and Snyder, H. S., 1958, Theory of the alternating-gradient synchrotron. *Ann. Phys.*, **3**, 1.

Crompvoets, F. M. H., Bethlem, H. L., Jongma, R. T., and Meijer, G., 2001, A prototype storage ring for neutral molecules. *Nature (London)*, **411**, 174.

Crompvoets, F. M. H., Jongma, R. T., Bethlem, H. L., van Roij, A. J. A., and Meijer, G., 2002, Longitudinal focusing and cooling of a molecular beam. *Phys. Rev. Lett.*, **89**, 093004.

Dahl, D. A., 1995, *Simion 3D*, Version 6.0 (Idaho Falls, Idaho National Engineering Laboratory).

Daussy, C., Marrel, T., Amy-Klein, A., Nguyen, C. T., Bordé, C. J., and Chardonnet, C., 1999, Limit on the parity nonconserving energy difference between the enantiomers of a chiral molecule by laser spetroscopy. *Phys. Rev. Lett.*, **83**, 1554.

deCarvalho, R., Doyle, J. M., Friedrich, B., Guillet, T., Kim, J., Patterson, D., and Weinstein, J. D., 1999, Buffer-gas loaded magnetic traps for atoms and molecules: a primer. *Eur. J. Phys.*, **7**, 289.

DeMille, D., 2002, Quantum computation with trapped polar molecules. *Phys. Rev. Lett.*, **88**, 067901.

DeMille, D., Bay, F., Bickman, S., Kawall, D., Krause Jr, D., Maxwell, S. E., and Hunter, L. R., 2000, Investigation of PbO as a system for measuring the electric dipole moment of the electron. *Phys. Rev.* A, **61**, 052507.

Donley, E. A., Claussen, N. R., Thompson, S. T., and Wieman, C. E., 2002, Atom–molecule coherence in a Bose–Einstein condensate. *Nature (London)*, **417**, 529.

Doyle, J. M., Friedrich, B., Kim, J., and Patterson, D., 1995, Buffer-gas loading of atoms and molecules into a magnetic trap. *Phys. Rev.* A, **52**, R2515.

Drag, C., Laburthe Tolra, B., Dulieu, O., Comparat, D., Vatasescu, M., Boussen, S., Guibal, S., Crubellier, A., and Pillet, P., 2000, Experimental versus theoretical rates for photoassociation and for formation of ultracold molecules. *IEEE J. quantum Electron.*, **36**, 1378.

Edwards, D. A., and Syphers, M. J., 1993, *An Introduction to the Physics of High Energy Accelerators* (New York, Wiley).

Egorov, D., Weinstein, J. D., Patterson, D., Friedrich, B., and Doyle, J. M., 2001, Spectroscopy of laser-ablated buffer-gas-cooled PbO at 4 K and the prospects for measuring the electric dipole moment of the electron. *Phys. Rev.* A, **63**, 030501(R).

Egorov, D., Lahaye, T., Schöllkopf, W., Friedrich, B., and Doyle, J. M., 2002, Buffer-gas cooling of atomic and molecular beams. *Phys. Rev.* A, **66**, 043401.

Field, R. W., Tilford, S. G., Howard, R. A., and Simmons, J. D., 1972, Fine structure and pertubation analysis of the $a^3\pi$ state of CO. *J. mol. Spectrosc.*, **44**, 347.

Fioretti, A., Comparat, D., Crubellier, A., Dulieu, O., Masnou-Seeuws, F., and Pillet, P., 1998, Formation of cold Cs_2 molecules through photoassociation. *Phys. Rev. Lett.*, **80**, 4402.

Friedburg, H., and Paul, W., 1950, Reflexion eines Atomstrahles am Rande eines Magnetfeldes. *Naturwissenschaften*, **37**, 20; 1951, Optische Abbildung mit neutralen Atomen. *Naturwissenschaften*, **38**, 159.

Friedrich, B., 2000, Slowing of supersonically cooled atoms and molecules by time-varying nonresonant induced dipole forces. *Phys. Rev.* A, **61**, 025403.

Friedrich, B., and Herschbach, D. R., 1991, On the possibility of orienting rotationally cooled polar molecules in an electric field. *Z. Phys.* D, **18**, 153; 1998, Space quantization: Otto Stern's lucky star. *Daedalus*, **127**, 165.

Friedrich, B., deCarvalho, R., Kim, J., Patterson, D., Weinstein, J. D., and Doyle, J. M., 1998, Towards magnetic trapping of molecules. *J. Chem. Soc., Faraday Trans.*, **94**, 1783.

Gabbanini, C., Fioretti, A., Lucchesini, A., Gozzini, S., and Mazzoni, M., 2000, Cold rubidium molecules formed in a magneto-optical trap. *Phys. Rev. Lett.*, **84**, 2814.

Gandhi, S. R., and Bernstein, R. B., 1987, Focusing and state selection of NH_3 and OCS by the electrostatic hexapole via first- and second-order Stark effects. *J. chem. Phys.*, **87**, 6457.

Gerton, J. M., Strekalov, D., Prodan, I., and Hulet, R. G., 2000, Direct observation of growth and collapse of a Bose–Einstein condensate with attractive interactions. *Nature (London)*, **408**, 692.

Golub, R., 1967, On decelerating molecules. PhD thesis, Massachusetts Institute of Technology.

Góral, K., Rzążewski, K., and Pfau, T., 2000, Bose–Einstein condensation with magnetic dipole–dipole forces. *Phys. Rev.* A, **61**, 051601(R).

Góral, K., Santos, L., and Lewenstein, M., 2002, Quantum phases of dipolar bosons in optical lattices. *Phys. Rev. Lett.*, **88**, 170406.

Gordon, J. P., Zeiger, H. J., and Townes, C. H., 1954, Molecular microwave oscillator and new hyperfine structure in the microwave spectrum of NH_3. *Phys. Rev.*, **95**, 282; 1955, The MASER—new type of microwave amplifier, frequency standard, and spectrometer. *Phys Rev*, **99**, 1264.

Goss Levi, B., 2000, Hot prospects for ultracold molecules. *Phys. Today*, **53**, 46.

Gould, H., 2000, Slowing, storing and cooling neutral molecules with synchrotrons. In *Book of Abstracts*, US DOE BES 2000 Meeting of the AMOP Program.

Greiner, M., Mandel, O., Esslinger, T., Hänsch, T. W., and Bloch, I., 2002, Quantum phase transition from a superfluid to a Mott insulator in a gas of ultracold atoms. *Nature (London)*, **415**, 39.

Günther, F., and Schügerl, K., 1972, State selection of polar molecules by alternate gradient focussing. *Z. Phys. Chem., N.F.*, **80**, 155.

GUPTA, M., and HERSCHBACH, D., 1999, A mechanical means to produce intense beams of slow molecules. *J. phys. Chem.* A, **103**, 10670; 2001, Slowing and speeding molecular beams by means of a rapidly rotating source. *J. phys. Chem.* A, **105**, 1626.

HARLAND, P. W., HU, W.-P., VALLANCE, C., and BROOKS, P. R., 1999, Spatial deorientation of upper-Stark-state-selected supersonic beams of CH_3F, CH_3Cl, CH_3Br, and CH_3I. *Phys. Rev.* A, **60**, 3138.

HEIJMEN, T. G. A., MOSZYNSKI, R., WORMER, P. E. S., VAN DER AVOIRD, A., RUDERT, A. D., HALPERN, J. B., MARTIN, J., BIN GAO, W., and ZACHARIAS, H., 1999, Rotational state-to-state rate constants and pressure broadening coefficients for He–C_2H_2 collisions: theory and experiment. *J. chem. Phys.*, **111**, 2519.

HEINZEN, D. J., RYU, C., COMPARAT, D., FREELAND, R. S., SHIM, W., VAN KEMPEN, E. G. M., KOKKELMANS, S. J. J. M. F., and VERHAAR, B. J., 2002, Magnetic trapping, collisions, and spectroscopy of ultracold Rb_2 molecules. In *Book of Abstracts, Cold Molecules and Bose–Einstein Condensation*, Les Houches, France.

HELMER, J. C., JACOBUS, F. B., and STURROCK, P. A., 1960, Focusing molecular beams of NH_3. *J. appl. Phys.*, **31**, 458.

HERSCHBACH, D., 1999, Chemical physics: molecular clouds, clusters, and corrals. *Rev. mod. Phys.*, **71**, S411.

HERSCHBACH, N., TOL, P. J. J., VASSEN, W., HOGERVORST, W., WOESTENENK, G., THOMSEN, J. W., VAN DER STRATEN, P., and NIEHAUS, A., 2000, Photoassociation spectroscopy of cold He(2^3S) atoms. *Phys. Rev. Lett.*, **84**, 1874.

HINDS, E. A., and SAUER, B. E., 1997, Probing TeV physics with feV interactions. *Phys. World*, **10**(4), 37.

HUDSON, J. J., SAUER, B. E., TARBUTT, M. R., and HINDS, E. A., 2002, Measurement of the electron electric dipole moment using YbF molecules. *Phys. Rev. Lett.*, **89**, 023003.

HUMPHRIES JR, S., 1986, *Principles of Charged Particle Acceleration* (New York: Wiley).

HUNTER, L. R., 1991, Tests of time-reversal invariance in atoms, molecules, and the neutron. *Science*, **252**, 73.

JONES, T., 2000, *Splitting the Second: The Story of Atomic Time* (Bristol: Institute of Physics Publishing).

JONGMA, R. T., 1997, Molecular beam experiments and scattering studies with state-selected metastable CO. PhD thesis, University of Nijmegen.

JONGMA, R. T., VON HELDEN, G., BERDEN, G., and MEIJER, G., 1997a, Confining CO molecules in stable orbits. *Chem. Phys. Lett.*, **270**, 304.

JONGMA, R. T., BERDEN, G., and MEIJER, G., 1997b, State-specific lifetime determination of the $a^3\pi$ state in CO. *J. chem. Phys.*, **107**, 1925.

KAKATI, D., and LAINÉ, D. C., 1967, Alternate-gradient focusing of a molecular beam of ammonia. *Phys. Lett.* A, **24**, 676; 1969, Alternate-gradient focusing of neutral particles. *Phys. Lett.* A, **28**, 786; 1971, Alternate-gradient focusing of a molecular beam. *J. Phys.* E, **4**, 269.

KATZ, D. P., 1997, A storage ring for polar molecules. *J. chem. Phys.*, **107**, 8491.

KAZACHOK, V. S., 1965, The electrodynamic method of slowing down molecules. *Sov. Phys. tech. Phys.*, **10**, 882.

KETTERLE, W., and PRITCHARD, D. E., 1992, Trapping and focusing ground state atoms with static fields. *J. Appl. Phys.* B, **54**, 403.

KETTERLE, W., and VAN DRUTEN, N. J., 1996, Evaporative cooling of trapped atoms. *Adv. at., mol., opt. Phys.*, **37**, 181.

KIM, J., FRIEDRICH, B., KATZ, D. P., PATTERSON, D., WEINSTEIN, J. D., DECARVALHO, R., and DOYLE, J. M., 1997, Buffer-gas loading and magnetic trapping of atomic europium. *Phys. Rev. Lett.*, **78**, 3665.

KING, J. G., 1959, Experiments with slow molecules. In *Proceedings of the 13th Annual Symposium on Frequency Control, Asbury Park*, US Army Signal Research and Development Laboratory, p. 603.

KING, J. G., and ZACHARIAS, J. R., 1958, Quarterly Progress Report, Vol. 48, 15 January 1958, Research Laboratory of Electronics, Massachusetts Institute of Technology.

Kokkelmans, S. J. J. M. F., Vissers, H. M. J., and Verhaar, B. J., 2001, Formation of a Bose condensate of stable molecules via a Feshbach resonance. *Phys. Rev.* A, **63**, 031601(R).

Kügler, K. J., Paul, W., and Trinks, U., 1978, A magnetic storage ring for neutrons. *Phys. Lett.* B, **72**, 422.

Laburthe Tolra, B., Drag, C., and Pillet, P., 2001, Formation of cold state-selected cesium molecules formed by stimulated Raman photoassociation. *Phys. Rev.* A, **64**, 061401(R).

Lainé, D. C., and Sweeting, R. C., 1973, Space focusing of molecules with a negative slope Stark interaction. *Entropie*, **42**, 165.

Latham, R. V., 1981, *High Voltage Vacuum Insulation: The Physical Basis* (London: Academic Press).

Letokhov, V. S., 1975, On difference of energy levels of left and right molecules due to weak interactions. *Phys. Lett.* A, **53**, 275.

Lett, P. D., Helmerson, K., Philips, W. D., Ratliff, L. P., Rolston, S. L., and Wagshul, M. E., 1993, Spectroscopy of Na_2 by photoassociation of laser-cooled Na. *Phys. Rev. Lett.*, **71**, 2200.

Li, H., Franks, K. J., Hanson, R. J., and Kong, W., 1998, Brute force orientation and alignment of Pyridazine probed by resonantly enhanced multiphoton ionization. *J. phys. Chem.* A, **102**, 8084.

Lichtenberg, A. J., 1969, *Phase-Space Dynamics of Particles* (New York: Wiley).

Livingood, J. J., 1961, *Principles of Cyclic Particle Accelerators* (New Jersey: van Nostrand).

Loesch, H.-J., 1996, A novel simple rotational state analyser/selector for polar linear molecules. *Chem. Phys.*, **207**, 427.

Loesch, H.-J., and Remscheid, A., 1990, Brute force in molecular reaction dynamics: a novel technique for measuring steric effects. *J. chem. Phys.*, **93**, 4779.

Loesch, H.-J., and Scheel, B., 2000, Molecules on Kepler orbits: an experimental study. *Phys. Rev. Lett.*, **85**, 2709.

Lovelace, R. V. E., Mehanian, C., Tommila, T. J., and Lee, D. M., 1985, Magnetic confinement of a neutral gas. *Nature (London)*, **318**, 30.

Lübbert, A., Günther, F., and Schügerl, K., 1975, Focusing of polar molecules in an alternate gradient focusing system. *Chem. Phys. Lett.*, **35**, 210.

Lübbert, A., Rotzoll, G., and Günther, F., 1978, Molecular beam focusing of ICl in rotational states with positive induced electric dipole moments. *J. chem. Phys.*, **69**, 5174.

Luiten, O. J., Reynolds, M. W., and Walraven, J. T. M., 1996, Kinetic theory of the evaporative cooling of a trapped gas. *Phys. Rev.* A, **53**, 381.

Maddi, J. A., Dinneen, T. P., and Gould, H., 1999, Slowing and cooling molecules and neutral atoms by time-varying electric-field gradients. *Phys. Rev.* A, **60**, 3882.

Maréchal, E., Guibal, S., Bossenec, J.-L., Barbé, R., Keller, J.-C., and Gorceix, O., 1999, Longitudinal focusing of an atomic cloud using pulsed magnetic forces. *Phys. Rev.* A, **59**, 4636.

Masnou-Seeuws, F., and Pillet, P., 2001, Formation of ultracold molecules ($T \leqslant 200\,\mu K$) via photoassociation in a gas of laser-cooled atoms. *Adv. At. mol. opt. Phys.*, **47**, 53.

McKenzie, C., Hecker Denschlag, J., Häffner, H., Browaeys, A., de Araujo, L. E. E., Fatemi, F. K., Jones, K. M., Simsarian, J. E., Cho, D., Simoni, A., Tiesinga, E., Julienne, P. S., Helmerson, K., Lett, P. D., Rolston, S. L., and Phillips, W. D., 2002, Photoassociation of sodium in a Bose–Einstein condensate. *Phys. Rev. Lett.*, **88**, 120403.

McMillan, E. M., 1945, The synchrotron—A proposed high energy particle accelerator. *Phys. Rev.*, **68**, 143.

Metcalf, H. J., and van der Straten, P., 1999, Laser cooling and trapping. (New York: Springer).

Migdall, A. L., Prodan, J. V., Phillips, W. D., Bergeman, T. H., and Metcalf, H. J., 1985, First observation of magnetically trapped neutral atoms. *Phys. Rev. Lett.*, **54**, 2596.

Miller, D. R., 1988, Free jet sources. In *Atomic and Molecular Beam Methods*, Vol I, edited by G. Scoles (New York: Oxford University Press), p. 14.

MILLER, J. D., CLINE, R. A., and HEINZEN, D. J., 1993, Photoassociation spectrum of ultracold Rb atoms. *Phys. Rev. Lett.*, **71**, 2204.

MODUGNO, G., FERRARI, G., ROATI, G., BRECHA, R. J., SIMONI, A., and INGUSCIO, M., 2001, Bose–Einstein condensation of potassium atoms by sympathetic cooling. *Science*, **294**, 1320.

MOSK, A. P., REYNOLDS, M. W., HIJMANS, T. W., and WALRAVEN, J. T. M., 1999, Photoassociation of spin-polarized hydrogen. *Phys. Rev. Lett.*, **82**, 307.

NIEL, L., and RAUCH, H., 1989, Acceleration, deceleration and monochromatization of neutrons in time dependent magnetic fields. *Z. Phys.* B, **74**, 133.

NIKOLOV, A. N., EYLER, E. E., WANG, X. T., LI, J., WANG, H., STWALLEY, W. C., and GOULD, P. L., 1999, Observation of ultracold ground-state potassium molecules. *Phys. Rev. Lett.*, **82**, 703.

NIKOLOV, A. N., ENSCHER, J. R., EYLER, E. E., WANG, H., STWALLEY, W. C., and GOULD, P. L., 2000, Efficient production of ground-state potassium molecules at sub-mK temperatures by two-step photoassociation. *Phys. Rev. Lett.*, **84**, 246.

ORAEVSKIĬ, A. N., 1964, *Molecular Generators* (Moscow: Nauka).

PAUL, W., 1990, Electromagnetic traps for charged and neutral particles. *Rev. mod. Phys.*, **62**, 531.

PEIK, E., 1999, Electrodynamic trap for neutral atoms. *Eur. Phys. J.* D, **6**, 179.

PHILLIPS, W. D., 1998, Nobel lecture: laser cooling and trapping of neutral atoms. *Rev. mod. Phys.*, **70**, 721.

PRESS, W. H., FLANNERY, B. P., TEUKOLSKY, S. A., and VETTERLING, W. T., 1986, *Numerical Recipes* (Cambridge: Cambridge University Press).

REGAN, B. C., COMMINS, E. D., SCHMIDT, C. J., and DEMILLE, D., 2002, New limit on the electron electric dipole moment. *Phys. Rev. Lett.*, **88**, 071805.

REIF, F., 1965, *Fundamentals of Statistical and Thermal Physics* (Singapore: McGraw-Hill).

REIN, D. W., 1974, Some remarks on parity violating effects of intramolecular interactions. *J. mol. Evol.*, **4**, 15.

REUSS, J., 1988, State selection by nonoptical methods. In *Atomic and Molecular Beam Methods*, Vol I, edited by G. Scoles (New York: Oxford University Press), p. 276.

SANDARS, P. G. H., 1965, The electric dipole moment of an atom. *Phys. Lett.*, **14**, 194.

SANTOS, L., SHLYAPNIKOV, G. V., ZOLLER, P., and LEWENSTEIN, M., 2000, Bose–Einstein condensation in trapped dipolar gases. *Phys. Rev. Lett.*, **85**, 1791.

SAUER, B. E., WANG, J., and HINDS, E. A., 1996, Laser-rf double resonance spectroscopy of ^{174}YbF in the $X^2\Sigma^+$ state: spin-rotation, hyperfine interactions, and the electric dipole moment. *J. chem. Phys.*, **105**, 7412.

SCHIFF, L. I., 1963, Measurability of nuclear electric dipole moments. *Phys. Rev.* A, **132**, 2194.

SCHLÖDER, U., SILBER, C., and ZIMMERMANN, C., 2001, Photoassociation of heteronuclear lithium. *Appl. Phys.* B, **73**, 801.

SCHREEL, K., SCHLEIPEN, J., EPPINK, A., and TER MEULEN, J. J., 1993, State-to-state cross sections for rotational excitation of OH by collisions with He and Ar. *J. chem. Phys.*, **99**, 8713.

SEKATSKIĬ, S. K., 1995, Electrostatic traps for polar molecules. *JETP Lett.*, **62**, 916.

SEKATSKII, S. K., and SCHMIEDMAYER, J., 1996, Trapping polar molecules with a charged wire. *Eur. Phys. Lett.*, **36**, 407.

SHAFFER, J. P., CHALUPCZAK, W., and BIGELOW, N. P., 1999, Photoassociative ionization of heteronuclear molecules in a novel two-species magneto-optical trap. *Phys. Rev. Lett.*, **82**, 1124.

SHIMIZU, F., and MORINAGA, M., 1992, Electric trapping of neutral atoms. *Jpn. J. appl. Phys.*, **31**, L1721.

SHLYAPNIKOV, G. V., 2001, private communication.

TAKEKOSHI, T., PATTERSON, B. M., and KNIZE, R. J., 1998, Observation of optically trapped cold cesium molecules. *Phys. Rev. Lett.*, **81**, 5105.

THORSHEIM, H. R., WEINER, J., and JULIENNE, P. S., 1987, Laser-induced photoassociation of ultracold sodium atoms. *Phys. Rev. Lett.*, **58**, 2420.

TRUSCOTT, A. G., STRECKER, K. E., MCALEXANDER, W. I., PARTRIDGE, G. B., and HULET, R. G., 2001, Observation of Fermi pressure in a gas of trapped atoms. *Science*, **291**, 2570.

van de Meerakker, S. Y. T., Jongma, R. T., Bethlem, H. L., and Meijer, G., 2001, *Accumulating NH radicals in a magnetic trap*. *Phys. Rev.* A, **64**, 041401(R).

Vanhaecke, N., de Souza Melo, W., Laburthe Tolra, B., Comparat, D., and Pillet, P., 2002, Accumulation of cold cesium molecules via photoassociation in a mixed atomic and molecular trap. *Phys. Rev. Lett.*, **89**, 063001.

Veksler, V., 1945, A new method of acceleration of relativistic particles. *J. Phys. (USSR)*, **9**, 153.

Webb, J. K., Murphy, M. T., Flambaum, V. V., Dzuba, V. A., Barrow, J. D., Churchill, C. W., Prochaska, J. X., and Wolfe, A. M., 2001, Further evidence for cosmological evolution of the fine structure constant. *Phys. Rev. Lett.*, **87**, 091301.

Weinstein, J. D., deCarvalho, R., Guillet, T., Friedrich, B., and Doyle, J. M., 1998a, Magnetic trapping of calcium monohydride molecules at millikelvin temperatures. *Nature (London)*, **395**, 148.

Weinstein, J. D., deCarvalho, R., Kim, J., Patterson, D., Friedrich, B., and Doyle, J. M., 1998b, Magnetic trapping of atomic chromium. *Phys. Rev.* A, **57**, R3173.

Wing, W. H., 1980, Electrostatic trapping of neutral atomic particles. *Phys. Rev. Lett.*, **45**, 631; 1984, On neutral particle trapping in quasistatic electromagnetic fields. *Prog. Quantum Electron.*, **8**, 181.

Wolfgang, R., 1968, Chemical accelerators. *Sci. Am.*, **219**(4), 44.

Wynar, R., Freeland, R. S., Han, D. J., Ryu, C., and Heinzen, D. J., 2000, Molecules in a Bose–Einstein condensate. *Science*, **287**, 1016.

Xu, G., 2001, Manipulation and quantum control of ultracold atoms and molecules for precision measurements. PhD thesis, The University of Texas at Austin.

Ye, J., 2002, private communication.

Zinner, G., Binnewies, T., Riehle, F., and Tiemann, E., 2000, Photoassociation of cold Ca atoms. *Phys. Rev. Lett.*, **85**, 2292.

Ziskind, M., Marrel, T., Daussy, C., and Chardonnet, C., 2002, Improved sensitivity in the search for a parity-violating energy difference in the vibrational spectrum of the enantiomers of CHFClBr. *Eur. Phys. J.* D, **20**, 219.

Zoller, P., 2002, Making it with molecules. *Nature (London)*, **417**, 493.